Bioconjugate Chemistry

Article

[213Bi]Bi3+/[111In]In3+-neunpa-cycMSH: Theranostic Radiopharmaceutical Targeting Melanoma—Structural, Radiochemical, and Biological Evaluation

Luke Wharton, Chengcheng Zhang, Hua Yang, Jutta Zeisler, Valery Radchenko,
Cristina Rodríguez-Rodríguez, Maryam Osooly, Brian O. Patrick, Kuo-Shyan Lin, François Bénard,
Paul Schaffer, and Chris Orvig*

Cite This: https://doi.org/10.1021/acs.bioconjchem.2c00038

Read Online

ACCESS | Metrics & More | Article Recommendations | Supporting Information

ABSTRACT: With the emergence of $[^{225}Ac]Ac^{3+}$ as a therapeutic radionuclide for targeted α therapy (TAT), access to clinical quantities of the potent, short-lived α-emitter $[^{213}Bi]Bi^{3+}$ ($t_{1/2}$ = 45.6 min) will increase over the next decade. With this in mind, the nonadentate chelator, H_4neunpa-NH$_2$, has been investigated as a ligand for chelation of $[^{213}Bi]Bi^{3+}$ in combination with $[^{111}In]In^{3+}$ as a suitable radionuclidic pair for TAT and single photon emission computed tomography (SPECT) diagnostics. Nuclear magnetic resonance (NMR) spectroscopy was utilized to assess the coordination characteristics of H_4neunpa-NH$_2$ on complexation of $[^{nat}Bi]Bi^{3+}$, while the solid-state structure of $[^{nat}Bi][Bi(neunpa-NH_3)]$ was characterized via X-ray diffraction (XRD) studies, and density functional theory (DFT) calculations were performed to elucidate the conformational geometries of the metal complex in solution. H_4neunpa-NH$_2$ exhibited fast complexation kinetics with $[^{213}Bi]Bi^{3+}$ at RT achieving quantitative radiolabeling within 5 min at 10^{-8} M ligand concentration, which was accompanied by the formation of a kinetically inert complex. Two bioconjugates incorporating the melanocortin 1 receptor (MC1R) targeting peptide Nle-CycMSH$_{hex}$ were synthesized featuring two different covalent linkers for *in vivo* evaluation with $[^{213}Bi]Bi^{3+}$ and $[^{111}In]In^{3+}$. High molar activities of 7.47 and 21.0 GBq/μmol were achieved for each of the bioconjugates with $[^{213}Bi]Bi^{3+}$. SPECT/CT scans of the $[^{111}In]In^{3+}$-labeled tracer showed accumulation in the tumor over time, which was accompanied by high liver uptake and clearance via the hepatic pathway due to the high lipophilicity of the covalent linker. *In vivo* biodistribution studies in C57Bl/6J mice bearing B16-F10 tumor xenografts showed good tumor uptake (5.91% ID/g) at 1 h post-administration with $[^{213}Bi][Bi(neunpa-Ph-Pip-Nle-CycMSH_{hex})]$. This study demonstrates H_4neunpa-NH$_2$ to be an effective chelating ligand for $[^{213}Bi]Bi^{3+}$ and $[^{111}In]In^{3+}$, with promising characteristics for further development toward theranostic applications.
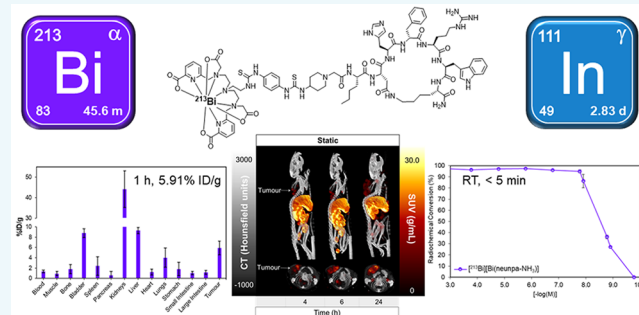
INTRODUCTION

The incidence of cutaneous melanoma has steadily increased over the past 30 years and is now currently ranked as the fifth most common form of cancer diagnosed in North America, accounting for an estimated 106,110 additional cases in the United States in 2021.[1] Although clinical intervention in localized disease is associated with 5-year relative survival rates of 94−97%, the prognosis for regional and distant metastatic disease is significantly worse (5-year relative survival: 65% and 25%, respectively).[2] With the advent of new therapeutic agents (immune check-point inhibitors, kinase inhibitors), significant improvements in the treatment of advanced-stage tumors has been achieved; however, recurrence of disease is still associated with poor patient outcomes (patient mortality) owing to the particularly aggressive metastatic power of cutaneous melanomas, and there is currently no FDA approved standard of care

for the treatment of metastatic uveal melanomas.[3−5] Suitable imaging agents are therefore essential for accurate staging of disease and determination of therapeutic efficacy.

Radiometal-based radiopharmaceutical agents are well established as effective prognostic tools for assessment of disease severity, staging progression, and evaluation of response to treatment within the oncology field.[6] In recent decades, the advent of peptide receptor radionuclide therapy (PRRT) in combination with targeted positron emission

Chart 1. Chemical Structures of Chelating Ligands Discussed
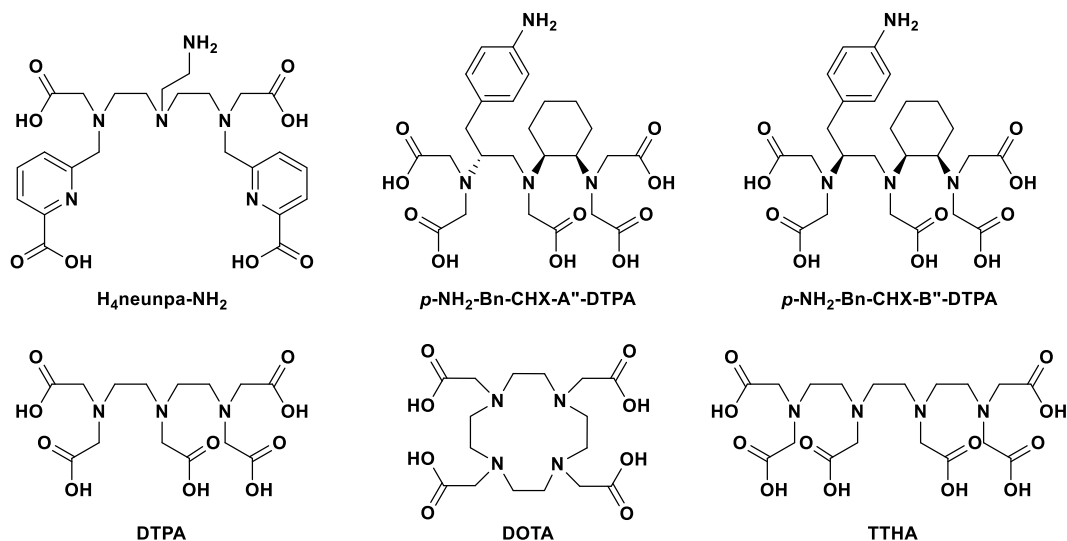
tomography (PET) and/or single photon emission computed tomography (SPECT) has seen the clinical approval of several peptide-based radiopharmaceutical agents, (e.g., [^{68}Ga]Ga-DOTATATE and [^{177}Lu]Lu-DOTATATE).[7,8]

To date, the most successfully applied therapeutic radiometals have featured β^--emitting radionuclides, such as ^{90}Y, ^{131}I, and ^{177}Lu, which have found particular utility for treatment of medium-sized, localized tumors.[9] However, recent efforts have now shifted focus toward α-emitting radionuclides, such as ^{225}Ac, ^{223}Ra, and ^{211}At, for combination in PRRT, due to their higher LET (80−100 keV/μm) and shorter effective range in tissue (40−100 μm) compared to β^--emitters,[10] which minimize the deleterious effects to surrounding nontarget tissues.[11−13] These characteristics result in a more localized delivery of dose and higher therapeutic potency, properties which are imperative for treatment of micrometastatic disease and single cell metastases.[6,11] Although several limitations have been noted, namely, low radiotracer stability (^{211}At-radiolabeled bioconjugates), limited treatment scope (^{223}RaCl$_2$; bone targeting), and difficulties in production (^{225}Ac). One attractive alternative is the short-lived theranostic radionuclide [^{213}Bi]Bi^{3+}, a potent α-emitter (E_α = 5.56−8.38 MeV) with imageable γ-ray emissions (79 and 440 keV),[14] suitable for concurrent SPECT diagnostics with dedicated high-energy collimators.[15] The short half-life of [^{213}Bi]Bi^{3+} ($t_{1/2}$ = 45.6 min) is particularly well-suited to the treatment of rapidly proliferating metastatic tumors and post-operative bacterial infections in combination with PRRT, due to the appropriate matching of radionuclidic half-life/cytotoxicity to the cell replication rate in these biological systems and the fast circulation and blood clearance characteristics of small peptide targeting vectors in vivo.[16] However, this aspect also poses a limitation, as the short-lived nature of this radionuclide may not be appropriate for treatment of slow-growing tumors or therapies involving slow accumulating target vectors (mAbs).

Melanocortin 1 receptor (MC1R) is a member of a family G-protein-coupled melanocortin receptors which is highly expressed in primary and metastatic melanomas, while low expression is reported in most normal human tissues; therefore, MC1R represents a viable target for selective imaging and therapy of metastasized melanomas.[17−19] Several radiotracers have been developed to target MC1R, which are

based on the endogenous α-melanocyte stimulating hormone (α-MSH), a nonselective agonist for MC1R with sub-nanomolar binding affinity (K_i = 0.23 nM).[20−26] Zhang et al. recently reported the introduction of ^{68}Ga-CCZ01048, a cyclic α-MSH analogue suitable for PET, with enhanced in vivo blood clearance, improved tumor uptake, and rapid cell internalization.[21]

The short half-life of [^{213}Bi]Bi^{3+} requires bifunctional chelating ligands which can achieve rapid (<10 min) quantitative radiolabeling at high molar activities under mild conditions (RT, physiological pH) to be compatible with biological targeting vectors, without the need for post-synthetic purification, characteristics not embodied by the current gold standard chelator DOTA (Chart 1). Human transferrin (hTF) is known to be a strong competitor for the Bi^{3+} ion (log K_1^* = 19.42, log K_2^* = 18.58), exhibiting a binding affinity comparable to the smaller metal ions Ga^{3+} (log K_1^* = 19.75, log K_2^* = 18.80) and In^{3+} (log K_1^* = 18.30, log K_2^* = 16.44); therefore, the formation of complexes with high thermodynamic stability is essential to prevent transchelation in vivo and subsequent kidney accumulation.[27,28]

Bi^{3+} is an intermediate hardness Lewis acidic metal ion, pK_a = 1.1, which typically forms stable coordination complexes with nitrogen-rich chelating ligands incorporating intermediate pyridine and picolinate donor groups.[29] The large ionic radius of Bi^{3+} (1.17 Å, CN = 8) favors metal complexes with high coordination numbers (8−9) with the most ubiquitous complexes featuring diethylenetriamine- and cyclen-based frameworks.[29] By far, the most applied chelating agent to date for Bi^{3+} is the non-macrocyclic ligand p-NH$_2$-Bn-CHX-A″-DTPA, Chart 1, which has found widespread application for evaluation of ^{213}Bi-radiolabeled monoclonal antibodies in vivo and has been featured in several Phase I and II clinical trials involving ^{213}Bi for treatment of acute myeloid leukemia (AML).[30,31] The acyclic framework of p-NH$_2$-Bn-CHX-A″-DTPA allows for facile radiolabeling kinetics, which is accompanied by high thermodynamic stability with Bi^{3+} (log K [Bi(CHX-A″-DTPA)]$^{2-}$ = 34.9).[28] Although [Bi(CHX-A″-DTPA)]$^{2-}$ has shown promise for clinical translation, the high anionic charge poses a major limitation, due to the influence on the pharmacokinetics and immunoreactivity of conjugated

Scheme 1. Synthetic Route for the Preparation of H$_4$neunpa-Ph-Pip-Nle-CycMSH$_{hex}$ (3) and Corresponding Bi^{3+} Cold Standard (4)
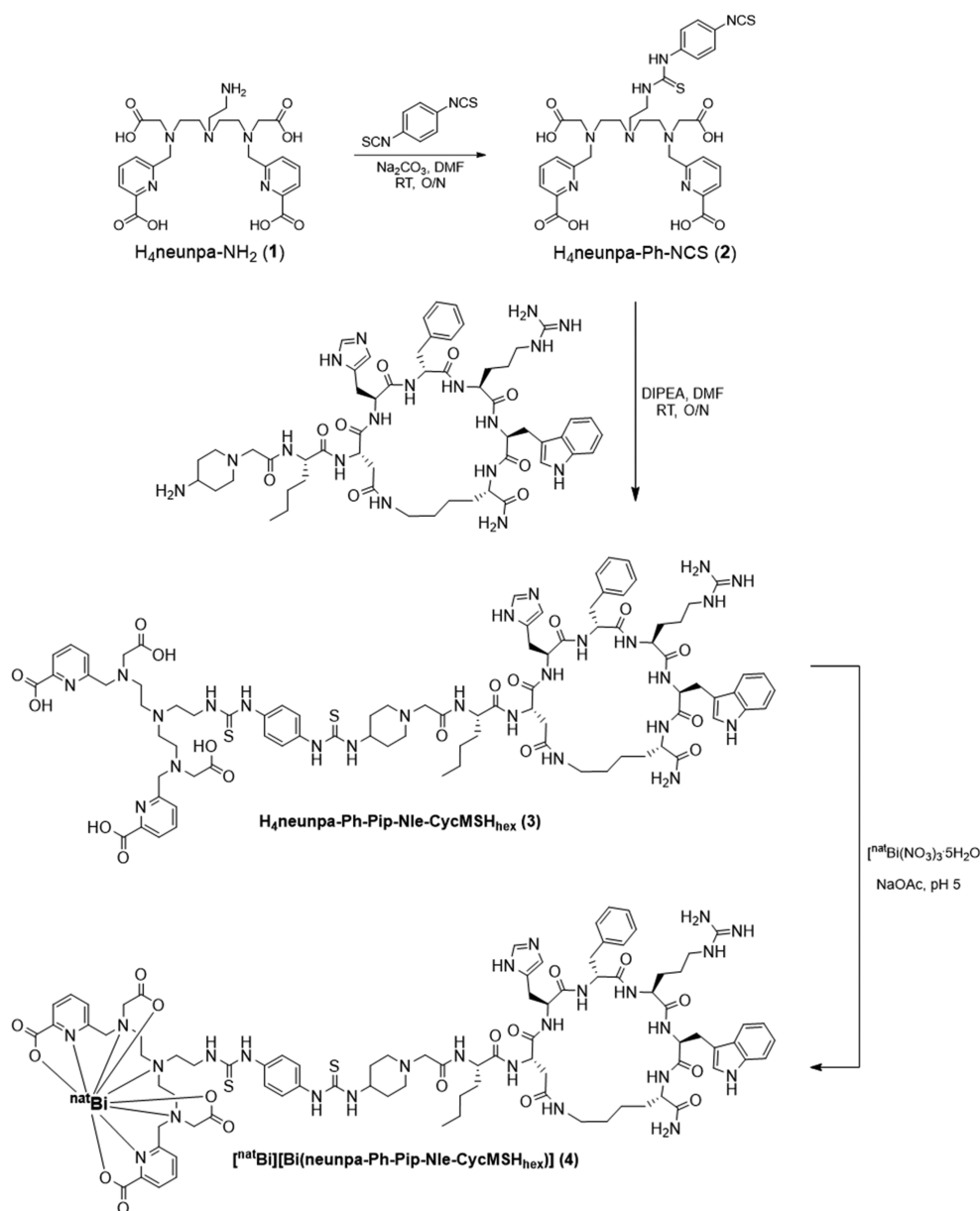
monoclonal antibodies, which diminishes the biological efficacy.[32−36]

Preceding work presented the coordination chemistry of the high denticity, bifunctional chelator, p-NO$_2$-Bn-H$_4$neunpa, with several trivalent metal ions, and noted the exceptionally high thermodynamic stability constant with Bi^{3+} (log K_{ML} = 28.76(9), pM = 27.0) which is comparable to $[Bi(DOTA)]^-$.[37] Following on was the report of an improved synthetic strategy with greater versatility toward bifunctionalization, which would allow broader application of this chelator to alternative targeting vectors.[38] Thus, with the above characteristics in mind, we now present the synthesis and evaluation of H$_4$neunpa-Ph-Pip-Nle-CycMSH$_{hex}$ and H$_4$neunpa-Ph-Aoc-Pip-Nle-CycMSH$_{hex}$ as theranostic radiopharmaceuticals for TAT/PRRT of MC1R positive melanomas with $[^{213}Bi]Bi^{3+}$ and $[^{111}In]In^{3+}$. To the best of our knowledge, this study encompasses the first in vivo evaluation combining $[^{213}Bi]Bi^{3+}$ and CycMSH$_{hex}$ for TAT.

■ RESULTS AND DISCUSSION

Synthesis. The bifunctional chelating ligand, H$_4$neunpa-NH$_2$, has been previously reported[37,38] and was synthesized following established procedures.[38] Preparation of H$_4$neunpa-Ph-Pip-Nle-CycMSH$_{hex}$ (3) was carried out in accordance with Scheme 1. First, the free primary amine of H$_4$neunpa-NH$_2$ (1) was coupled with p-phenylene diisothiocyanate under mildly basic conditions to yield the corresponding phenyl isothiocyanate (H$_4$neunpa-Ph-NCS) (2) which is suitable for direct conjugation with amine residues. Purification of H$_4$neunpa-Ph-NCS (2) was achieved using reverse-phase high-performance liquid chromatography (RP-HPLC), and the NCS functional group was coupled with H$_2$N-Pip-Nle-CycMSH$_{hex}$ to give the corresponding thiourea (3) in high yield. H$_4$neunpa-Ph-Pip-Nle-CycMSH$_{hex}$ (3) was purified via RP-HPLC and further analyzed using HR-ESI-MS used to confirm formation of the expected product. The nonradioactive $[^{nat}Bi]Bi^{3+}$ complex (4)

was prepared by addition of an equimolar amount of $Bi(NO_3)_3 \cdot 5H_2O$ to an aqueous solution of H_4neunpa-Ph-Pip-Nle-CycMSH$_{hex}$ at pH 5.0. RP-HPLC yielded the corresponding cold standard with high purity, and the molecular weight was verified using HR-ESI-MS (Table 1).

Table 1. Mass Spectrometry Analysis for αMSH Derivatives

| compound	theoretical mass [M + H]+	experimental mass [M + H]+
H_4neunpa-Ph-Pip-Nle-CycMSH$_{hex}$	1846.8351	1846.8427
[^{nat}Bi][Bi(neunpa-Ph-Pip-Nle-CycMSH$_{hex}$)]	2052.7904	2052.7978
H_4neunpa-Ph-Aoc-Nle-CycMSH$_{hex}$	1987.9501	1987.9573
[^{nat}In][In(neunpa-Ph-Aoc-Nle-CycMSH$_{hex}$)]	2099.8331	2099.8392

In the course of our investigations, it became apparent that the absence of a flexible covalent linkage between the chelator and the targeting vector led to partial inhibition of radiometal ion coordination, which would later impact the highest achievable molar activities. Hence, in order to overcome this limitation, a synthetic analogue of H_4neunpa-Ph-Pip-Nle-CycMSH$_{hex}$ with an elongated alkyl spacer (Aoc) between the chelator and Pip-Nle-CycMSH$_{hex}$ peptide was prepared, with enhanced radiolabeling characteristics. H_4neunpa-Ph-Aoc-Pip-Nle-CycMSH$_{hex}$ (**5**) was prepared using an analogous route to H_4neunpa-Ph-Pip-Nle-CycMSH$_{hex}$, wherein the NCS functional group of the ligand (**2**) was coupled to the free primary amine of H_2N-Aoc-Pip-Nle-CycMSH$_{hex}$ (Scheme 2). The modified H_2N-Aoc-Pip-Nle-CycMSH$_{hex}$ peptide was synthesized via solid-phase peptide synthesis using the same approach previously reported for CCZ01048;[21] however, the amino acid sequence was further extended by coupling of Fmoc-Aoc-CO$_2$H to the piperidine prior to cyclization, deprotection, and cleavage from the resin. Isolation of (**5**)

Scheme 2. Synthetic Route for the Preparation of H_4neunpa-Ph-Aoc-Pip-Nle-CycMSH$_{hex}$ (5) and Corresponding In^{3+} Cold Standard (6)
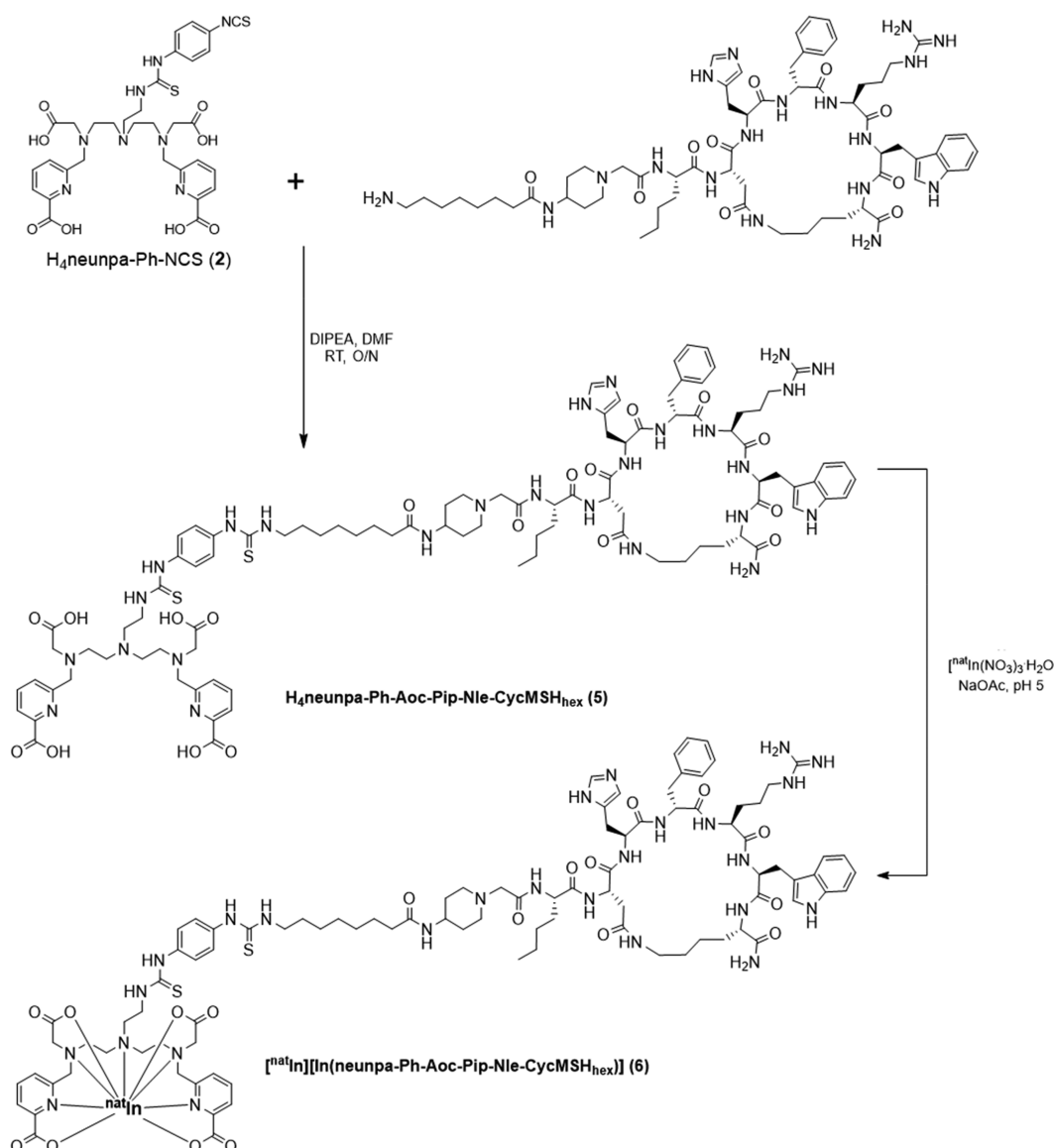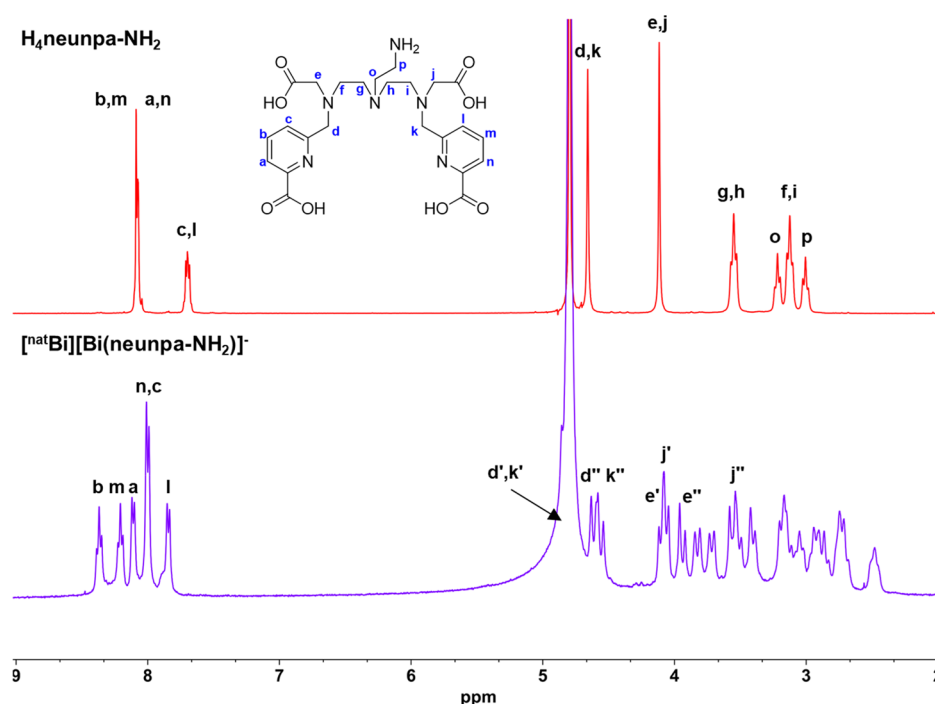
Figure 1. Stacked ^{1}H NMR spectra of H$_4$neunpa-NH$_2$ (red) and the corresponding complex with Bi^{3+} (purple); 400 MHz, D$_2$O, 298 K, pD 7.0.

was achieved using RP-HPLC, and the corresponding nonradioactive $[^{nat}In][In^{3+}$ complex (**6**) was prepared using the same approach as outlined for compound **4**. Confirmation of product isolation and purity was achieved using HPLC and HR-ESI-MS (Table 1).

The inhibition constant (K_i) of $[^{nat}Bi][Bi(neunpa-Ph-Pip-Nle-CycMSH_{hex})]$ toward MC1R was evaluated using competitive binding assays in the B16-F10 melanoma cell line. $K_i = 0.62$ (± 0.25) nM was determined for $[^{nat}Bi][Bi-(neunpa-Ph-Pip-Nle-CycMSH_{hex})]$, comparable to similar conjugates based on the Pip-Nle-CycMSH$_{hex}$ sequence and confirming that modification through the piperidine linker in this manner does not negatively impact receptor binding affinity.[20,21] Representative plots for the competitive binding assay are provided in Figure S18.

Metal Complexation and Characterization. To investigate the coordination characteristics of H$_4$neunpa-NH$_2$ with In^{3+} and Bi^{3+}, the corresponding metal complexes were prepared by addition of each respective metal nitrate salt to aqueous solutions of the ligand in a 1:1 molar ratio. The pH of the resulting mixtures was adjusted to neutral using NaOH solution (1.0 M) to attain a single dominant species, as determined by previous potentiometric–spectrophotometric titration studies. The metal complexes were isolated by filtration and lyophilized prior to reconstitution in D$_2$O for NMR characterization. Both complexes were characterized via high-resolution electrospray ionization mass spectrometry (HR-ESI-MS), high-performance liquid chromatography (HPLC), and NMR spectroscopy.

The NMR characterization of $[^{nat}In][In(neunpa-NH_2)]^-$ has been evaluated in detail previously[38] and revealed the formation of a single asymmetric complex in solution in which all four donor arms are strongly coordinated to the In^{3+} metal center (Figure S7). This assessment was supported through computational studies which indicated the predominance of a single isomer with an anti N$_1$^{R}N$_2$^{R}Λ($\lambda\delta$) configuration wherein

the picolinic acid donors coordinate on opposite faces of the metal and the central tertiary amine remains uncoordinated.

In the case of $[^{nat}Bi][Bi(neunpa-NH_2)]^-$, there is a decrease in spectral symmetry on complexation of Bi^{3+} in comparison to the "free" ligand, as evidenced by the aromatic region of the picolinate donor groups (Figure 1). Additionally, the methylenic protons adjacent to the picolinate (H$_d$/H$_k$) and acetate (H$_e$/H$_j$) pendent donor arms exhibit diastereotopic splitting, appearing as distinct AB doublets with large coupling constants ($^2J_{HH} = 15.5-18.5$ Hz), implying coordination to the Bi^{3+} metal center. Overall, the ^{1}H NMR spectrum of the $[^{nat}Bi][Bi(neunpa-NH_2)]^-$ complex reveals a single asymmetric species with distinct spectral features from that of the previously reported In^{3+} complex, specifically in terms of the chemical shifts of the methylene and aromatic protons. These differences may imply a change in the relative donor group configuration (i.e., syn vs anti) between each complex; however, it is difficult to surmise this based solely on this spectroscopic data. It is possible that these differences arise due to the different coordination characteristics of Bi^{3+} and In^{3+}. While both metal ions exhibit borderline chemical hardness with a preference for softer O and N donors,[39] Bi^{3+} is considerably larger than In^{3+} (1.17 Å vs 0.92 Å, respectively; CN = 8) with a more diffuse atomic charge and can attain higher-order monomeric structures in complexes with high denticity polyaminocarboxylate ligands (e.g., $([Bi(H_3ttha)]\cdot 3H_2O)$; CN = 10).[29,40] Furthermore, Bi^{3+} is known to exhibit a stereochemically active lone pair in some of its coordination complexes, which can significantly alter ligand conformation and donor atom coordination, an effect which is particularly evident with hard, ionic donor groups. Thus, a change in the effective denticity of H$_4$neunpa-NH$_2$ in each complex may contribute to the difference in preferred configuration/conformation as seen in the NMR spectra.

X-ray Crystallography. Single colorless prism-shaped X-ray quality crystals of $[Bi(neunpa-NH_3)]\cdot 2H_2O$ were obtained
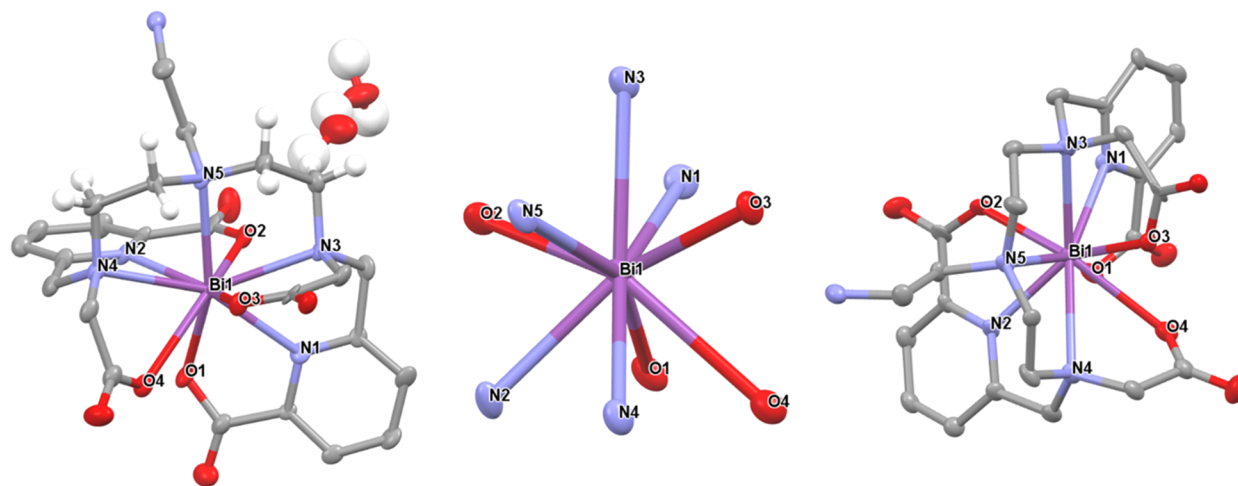
Figure 2. ORTEP diagrams of [Bi(neunpa-NH₃)]·2H₂O. Ellipsoids are shown at 50% probability; selected hydrogens and cocrystallized H$_2$O molecules have been omitted for clarity. The nine donor atoms comprising the nonadentate coordination sphere of Bi^{3+} are shown (center).

by slow evaporation from an aqueous solution containing Bi(NO$_3$)$_3$·5H$_2$O and H$_4$neunpa-NH$_2$·6HCl·3H$_2$O in a 1:1 molar ratio, adjusted to pH 5 using NaOH. X-ray diffraction measurements reveal that the complex crystallizes in the polar, non-centrosymmetric Pna2$_1$, orthorhombic space group, in which the asymmetric unit contains the [Bi(neunpa-NH$_3$)] molecule and two cocrystallized water molecules (Figure 2). Key bond distances for the metal coordination sphere are outlined in Table 2, and full crystallographic results are

Table 2. Selected Bond Lengths in Å for [Bi(neunpa-NH$_3$)]· 2H$_2$O

atom	atom	length/Å
Bi1	O1	2.544(9)
Bi1	O2	2.321(9)
Bi1	O3	2.501(8)
Bi1	O4	2.733(10)
Bi1	N1	2.584(8)
Bi1	N2	2.487(11)
Bi1	N3	2.631(11)
Bi1	N4	2.729(12)
Bi1	N5	2.614(12)

provided in the Supporting Information. The crystal structure shows an uncommon example of a nonadentate bismuth complex in which all nine donor atoms from the ligand are coordinated to the metal center.

The coordination environment around the central metal ion can be described as a distorted capped square antiprism wherein the two terminal amines in the backbone, N(3) and N(4), attain different absolute chiralities, giving rise to an overall syn conformation in which the two acetate donor groups, O(3) and O(4), are positioned on the same face of the metal. The metal coordination sphere shows a preferential binding toward the oxygen donors of the ligand over the nitrogen donors, wherein the Bi−O bond distances vary between 2.321 and 2.731 Å (average 2.525 Å) while the Bi−N bond distances are longer at 2.487−2.729 Å (2.609 Å). The shortest Bi−O and Bi−N bond lengths (2.321 and 2.487 Å, respectively) correspond to the carboxylate O(2) and pyridyl N(2) donors on the same picolinic acid, while the longest Bi−O and Bi−N bonds lengths (2.731 and 2.729 Å, respectively)

comprise the acetate O(4) and terminal nitrogen N(4) on the same side of the molecule. This is consistent with the NMR characterization of [Bi(neunpa-NH$_3$)] (Figure 1) which showed the methylene protons (H$_{j'/j''}$) on one acetate group in a less deshielded environment, implying weaker coordination the metal center and an elongated bond distance.

In comparison, the non-macrocyclic polyaminocarboxylate chelator H$_5$DTPA, which has been extensively studied for Bi^{3+} complexation, and its bifunctional analogue p-NH$_2$-Bn-CHX-A″-DTPA exhibit a distinctly different metal coordination environment. The solid-state structure of [Bi(H$_2$DTPA)]· 2H$_2$O is composed of a polymeric network wherein the ligand is coordinated in a heptadentate fashion to the metal ion, with the eighth coordination site occupied by an intermolecular bridging carbonyl oxygen donor from the ligand in a neighboring complex.[40,41] The reported Bi−O and Bi−N bond lengths of [Bi(H$_2$DTPA)]·2H$_2$O ((2.290−2.699 Å) and (2.449−2.723 Å), respectively) compare favorably to [Bi-(neunpa-NH$_3$)]; thus, the slow release of Bi^{3+} by DTPA observed in vivo is likely a result of the difference in the apparent denticity of the two ligands in solution.[28,42] As reported by Brechbiel et al., the enhanced rigidity imposed by the cyclohexyl moiety in [Bi(Cy-DTPA) reduces the lability of the metal complex in vivo although the metal coordination sphere remains unsaturated by the ligand (CN = 8).[41]

Computational Studies. The solution state structure of the neutral coordination complex [Bi(neunpa-NH$_3$)] was investigated using density functional theory (DFT) calculations, performed within the Gaussian 16 software package (Revision B.01) using the meta-generalized gradient approximation (meta-GGA) M06-2X functional, which has been shown to be effective for modeling of main group metal ions including Bi^{3+} and Pb^{2+}.[43−45] Large-core relativistic effective core potentials (LCRECP) and the associated valence basis sets were used for modeling of Bi^{3+}, while light atoms (C, H, N, O) were treated up to Def2TZVP levels of theory.[43,46] The conformational isomers of [Bi(neunpa-NH$_3$)] were investigated through geometric optimizations in aqueous solution using the PCM solvation model and vibrational frequency analysis of their local energy minima.

The different conformational isomers of [Bi(neunpa-NH$_3$)] arise from (1) the absolute chirality of the tertiary amines within the backbone of the ligand (R or S) and (2) the relative

orientation of the five-membered chelate rings formed between the metal ion and the ligand framework (λ or δ) (Figure 3).
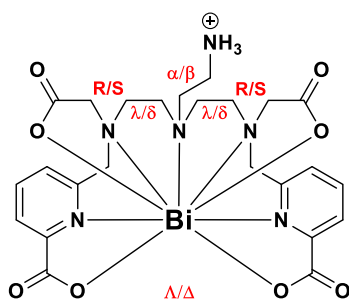
Figure 3. Depiction of the sources of chirality contributing to the different conformational isomers of [Bi(neunpa-NH$_3$)].

Collectively this gives rise to 12 possible diastereomers: 4 anti and 8 syn, based on the configuration of the central amine (α or β). Additionally, these diastereomers can attain different overall geometries based on the relative arrangement of donor arms (Λ or Δ), giving rise to a total of 20 possible conformational isomers with the same coordination number and linker orientation. Fully optimized structures are provided in Figures S29−S47.

Geometry optimizations of [Bi(neunpa-NH$_3$)] strongly indicate a preference for coordination in the syn α N$_1^S$N$_2^R$$\Lambda$-($\lambda\delta$) configuration, wherein the central alkyl linker is orientated above the plane of picolinate donor binding (Figure 4). Notably, this configuration is directly comparable to the experimentally derived structure determined via X-ray crystallography. Calculations of the relative free energy differences between the different conformers found the syn configuration to be more stable than the equivalent anti configuration by 9.2 kJ/mol, indicating the predominance of a single conformer in solution (Table 3). This large energy difference is consistent with experimental NMR results which showed the presence of a single asymmetric isomer in solution. Furthermore, the DFT optimized structure clearly reflects the anisotropic environment attained by the methylenic protons adjacent to the pendent donor arms, and thus the corresponding appearance of diastereotopic doublets in the ^{1}H NMR spectrum.

A notable feature captured by the DFT calculations is the preferential arrangement of the backbone chelate rings in the $\lambda\delta$ conformation, which appears as the lowest energy

Table 3. Relative Free Energy Differences between DFT Optimized Structures of [Bi(neunpa-NH$_3$)] Calculated at TZVP Levels of Theory

	conformation[a]	ΔE (kJ/mol)	ΔG (kJ/mol)
Anti configuration	N$_1^R$N$_2^R$ ($\lambda\delta$)	+9.67	+9.19
	N$_1^R$N$_2^R$ ($\lambda\lambda$)	+15.8	+17.2
	N$_1^R$N$_2^R$ ($\delta\lambda$)	+26.9	+23.8
	N$_1^R$N$_2^R$ ($\delta\delta$)	+22.7	+27.7
Syn configuration	α N$_1^R$N$_2^S$ Λ ($\lambda\delta$)	0	0
	α N$_1^R$N$_2^S$ Λ ($\lambda\lambda$)	+16.9	+17.4
	α N$_1^R$N$_2^S$ Λ ($\delta\lambda$)	+21.1	+18.8
	α N$_1^R$N$_2^S$ Λ ($\delta\delta$)	+29.5	+26.2
Syn configuration	β N$_1^R$N$_2^S$ Λ ($\lambda\delta$)	+43.8	+43.9
	β N$_1^R$N$_2^S$ Λ ($\lambda\lambda$)	+62.0	+61.0
	β N$_1^R$N$_2^S$ Λ ($\delta\lambda$)	+48.4	+46.7
	β N$_1^R$N$_2^S$ Λ ($\delta\delta$)	+82.5	+73.3
Syn configuration	α N$_1^R$N$_2^S$ Δ ($\lambda\delta$)	+27.1	+27.4
	α N$_1^R$N$_2^S$ Δ ($\lambda\lambda$)	+38.1	+34.3
	α N$_1^R$N$_2^S$ Δ ($\delta\lambda$)	+49.7	+48.0
	α N$_1^R$N$_2^S$ Δ ($\delta\delta$)	+75.0	+71.1
Syn configuration	β N$_1^R$N$_2^S$ Δ ($\lambda\delta$)	+62.7	+56.4
	β N$_1^R$N$_2^S$ Δ ($\lambda\lambda$)	+55.8	+51.1
	β N$_1^R$N$_2^S$ Δ ($\delta\lambda$)	+67.7	+61.8
	β N$_1^R$N$_2^S$ Δ ($\delta\delta$)	n/a	n/a[b]

[a]Notation: α/β: central amine configuration, N$_1^{R/S}$N$_2^{R/S}$: terminal amine configuration, Λ/Δ: acetate donor chirality, λ/δ: 5-membered chelate chirality. [b]Converged to give the same configuration as α N$_1^R$N$_2^S$ Δ ($\delta\delta$).

arrangement in the majority of possible isomers. This trend was also observed in studies of La^{3+}, Lu^{3+}, and In^{3+} complexes of H$_4$neunpa-NH$_3$ indicating an energetic preference to adopt a linear arrangement of the ethylene backbone bridges over a twisted/staggered orientation.[38]

Both the DFT-derived and X-ray crystallographic structures of [Bi(neunpa-NH$_3$)] show a small degree of asymmetry in the coordination sphere, wherein the Bi(1)−O(4) and Bi(1)−N(4) bond distances are elongated in comparison to the remaining donor atoms. This distortion may arise from the presence of a stereochemically active Bi^{3+} 6s^2 lone pair which influences the electron density in this region of the complex. To investigate this phenomenon, natural bond orbital (NBO) analysis was applied to the X-ray crystal structure of [Bi(neunpa-NH$_3$)] to assess the 6p contribution to the 6s^2 lone pair of the Bi^{3+} ion. This analysis indicated a small amount
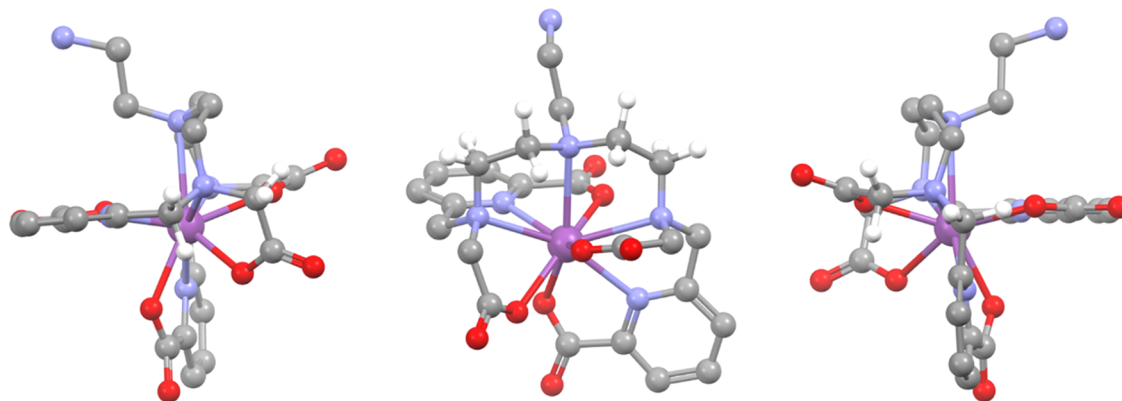
Figure 4. DFT optimized structures of [Bi(neunpa-NH$_3$)] in α N$_1^S$N$_2^R$ Λ ($\lambda\delta$) configuration. Selected hydrogens have been omitted for clarity.
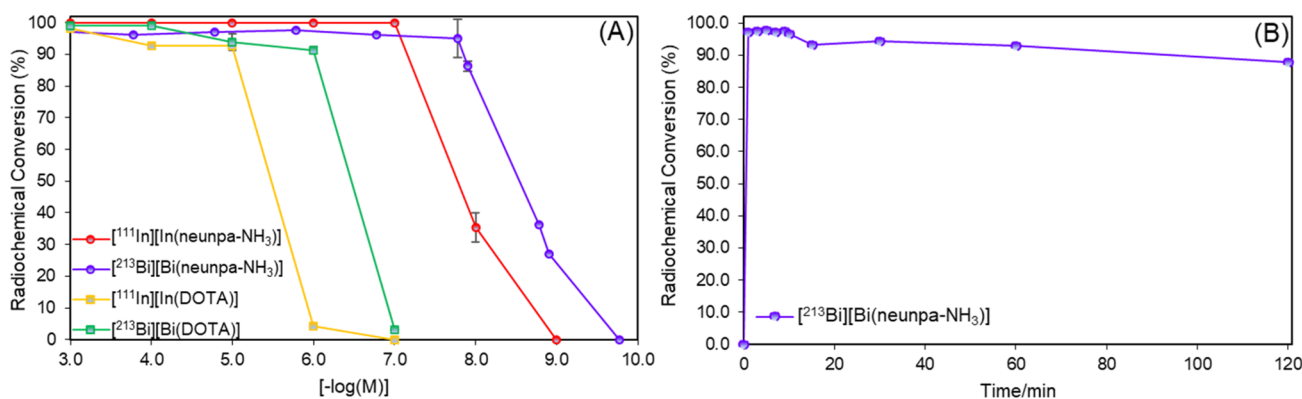
Figure 5. (A) Concentration-dependent radiolabeling of H_4neunpa-NH_3 and DOTA (note: radiolabeling performed at 85 °C over 30 min) with $[^{213}Bi]Bi^{3+}$ (650 kBq) and $[^{111}In]In^{3+}$ (1.30 MBq) performed at RT over 5–7 min; V_T = 100 μL. (B) Time-dependent radiolabeling of H_4neunpa-NH_2 (10 μL) with $[^{213}Bi]Bi^{3+}$ (650 kBq, 10 μL) performed at RT in MES buffer (0.5 M, pH 5.5, 30 μL).
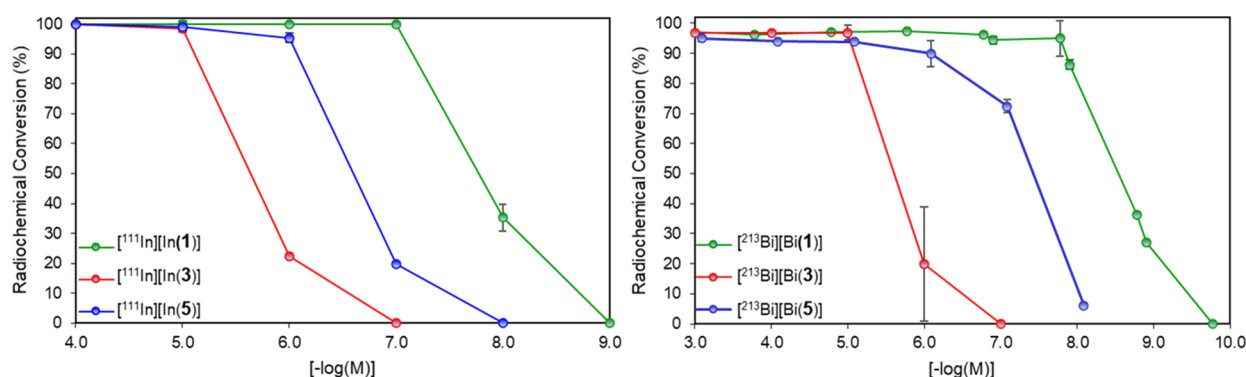
Figure 6. Concentration-dependent radiolabeling of H_4neunpa-NH_2 (**1**), H_4neunpa-Ph-Pip-Nle-CycMSH$_{hex}$ (**3**), and H_4neunpa-Aoc-Ph-Pip-Nle-CycMSH$_{hex}$ (**5**) with $[^{111}In]In^{3+}$ (1.0 MBq) and $[^{213}Bi]Bi^{3+}$ (650 kBq) at RT monitored over 10 min.

of 6p contribution (0.40%) to the $6s^2$ lone pair, thus implying a minor degree of polarization and a largely inactive $6s^2$ lone pair. Visualization of the MO containing the $6s^2$ lone pair shows a near-symmetric distribution of electron density, which is consistent with the NBO analysis (Figure S48). Hence, the asymmetry in the coordination environment is likely a result of the electrostatic and steric characteristics of the ligand rather than the metal ion; the particularly short bond distance between Bi(1) and O(2) consequently disfavors close binding of the neighboring acetate donor.

Radiolabeling Studies. The nuclear decay characteristics and chemical behavior of radionuclides associated with the $^{225}Ac/^{213}Bi$ generator have been thoroughly evaluated in previous studies, and as such, well-established methodologies encompassing generator preparation, optimal radionuclide equilibration times, elution profiles, and radiolabeling parameters have been determined.[47,48] $[^{213}Bi]Bi^{3+}$ can be produced using an $^{225}Ac/^{213}Bi$ generator system based on AG MP-50 cation exchange resin and is readily eluted with 0.1 M NaI/HCl solution in the form of $[BiI_4]^-$ and $[BiI_5]^{2-}$.[48] The short half-life of $[^{213}Bi]Bi^{3+}$ ($t_{1/2}$ = 45.6 min) and high radiolytic potency of its decay progeny, particularly attractive for therapeutic applications, requires the development of chelating ligands which demonstrate fast, quantitative radiolabeling kinetics (<5 min), ideally under mild conditions (RT, pH 5–8), which also maintain high kinetic inertness *in vivo*. The decay of $[^{213}Bi]Bi^{3+}$ proceeds through a series of short-lived daughter radionuclides, including the relatively long-lived isotope $[^{209}Pb]Pb^{2+}$ ($t_{1/2}$ = 3.3 h), a pure β^- emitter, followed

by subsequent decay to stable ^{209}Bi. Thus, to avoid complications in the radiochemical analysis of reaction mixtures containing $[^{213}Bi]Bi^{3+}$ and its daughter $[^{209}Pb]Pb^{2+}$, the radiochemical conversion (RCC) was determined by quantification of the 440 keV γ-emission line of $[^{213}Bi]Bi^{3+}$ using γ spectroscopy.

The suitability of H_4neunpa-NH_2 (as $[neunpa-NH_3]^{3-}$) to chelate $[^{213}Bi]Bi^{3+}$ was assessed in a series of radiolabeling experiments outlined in Figure 5. Concentration-dependent radiolabeling studies of H_4neunpa-NH_2 with $[^{213}Bi]Bi^{3+}$ revealed highly effective complexation, achieving quantitative radiochemical conversion (>96%) over a broad concentration range (10^{-3} to 10^{-8} M) under exceptionally mild conditions (5 min, RT). A corresponding ligand-to-metal ratio of 235:1 was achieved for $[^{213}Bi][Bi(neunpa-NH_3)]$.

The concentration dependence of $[^{213}Bi][Bi(neunpa-NH_3)]$ compares favorably to the corresponding $[^{111}In]In^{3+}$ radiolabeled complex, which has demonstrated highly effective chelation under mild conditions (>99% RCC at 10^{-7} M, 10 min, RT) with molar activities exceeding 164 MBq/nmol (L:M; 7:1).[38] The high radiochemical purity (RCP) of the $[^{111}In]In^{3+}$ and $[^{213}Bi]Bi^{3+}$ labeled complexes was confirmed by radio-HPLC (Figure S22); notably the radiolabeled complexes exhibited different retention times (8.34 and 6.99 min, respectively), supporting the assignment of a difference in geometric configuration (anti vs syn) between the two complexes. Collectively, these results highlight H_4neunpa-NH_2 as a potentially valuable tool for the use of $[^{111}In]In^{3+}$ and $[^{213}Bi]Bi^{3+}$ as a theranostic pair. By comparison, radiolabeling

H

studies conducted with DOTA in parallel show a markedly poorer ability to complex $[^{111}In]In^{3+}$ or $[^{213}Bi]Bi^{3+}$, with radiolabeling efficiencies being 2 orders of magnitude lower than for H_4neunpa-NH_2, even under the more aggressive conditions typically used for macrocycle labeling (>85 °C, 30−60 min).

The kinetics of metal complexation were investigated in a time-dependent radiolabeling study of H_4neunpa-NH_3 (Figure 5B), which revealed near-quantitative (96%) radiolabeling was achieved after <1 min at RT, and complete RCC was attained at 7 min after addition of $[^{213}Bi]Bi^{3+}$. The time-dependent study continued over 2 h to assess how the radiolabeling mixture develops throughout the first three half-lives of $[^{213}Bi]Bi^{3+}$. Measurements of the separated radiolabeled complex and "free" $[^{213}Bi]Bi^{3+}$ infer the kinetic inertness of the $[^{213}Bi][Bi(neunpa-NH_3)]$ complex, which remains >88% intact over a 2 h period. The small reduction in the integrity of $[^{213}Bi][Bi(neunpa-NH_3)]$ (<10% over 2 h) as measured by γ spectroscopy can be attributed to radiolysis within the reaction solution, whereby the coproduction of reactive radical species causes degradation of the surrounding complex molecules. This oxidative stress-induced degradation can be mitigated through the use of radiolysis quenchers such as sodium ascorbate or gentisic acid within the radiolabeling cocktail.[49]

The comparable affinity of H_4neunpa-NH_2 for $[^{111}In]In^{3+}$ and $[^{213}Bi]Bi^{3+}$ chelation was further observed in radiolabeling studies of the corresponding bioconjugate, H_4neunpa-Ph-Pip-Nle-CycMSH$_{hex}$ (3); however, notable reductions in the radiolabeling efficiency at low concentrations (10^{-6} and 10^{-7} M) were apparent (Figure 6). Optimization of the radiolabeling parameters through modification of the reaction temperature, time, pH, buffer, and additional cosolvents yielded no improvements to the RCC for either radionuclide. It is possible that the cationic piperidine linker contributes to the decrease in radiolabeling efficiency, due to its close proximity to the chelator binding cavity and its associated electrostatic repulsion. As the cationic piperidine motif has been shown to be beneficial for receptor uptake and blood clearance *in vivo*,[21] a modified construct was synthesized incorporating an 8-aminooctanyl spacer (Aoc) in addition to the cationic piperidine unit, with the aim of increasing separation between the chelating ligand and the targeting vector.

As is clearly evident from Figure 6, the installation of a longer covalent linkage between the chelator and targeting peptide improved the radiolabeling efficiency, whereby near quantitative RCCs were achieved at 10^{-6} M for both $[^{111}In]In^{3+}$ and $[^{213}Bi]Bi^{3+}$. These results are particularly significant for preclinical *in vivo* studies involving $[^{213}Bi]Bi^{3+}$ which require high molar activities to be achieved without post-radiolabeling purification (radio-HPLC, C18 SepPak) prior to administration.

A maximum molar activity of 21 MBq/nmol was achieved for $[^{213}Bi][Bi(neunpa-Ph-Pip-Nle-CycMSH_{hex})]$ with a RCP of >95% using 200 pmol of precursor (Figures S24−S25). This result is directly comparable to highest molar activities reported for $[^{213}Bi][Bi(DOTATATE)]$ (28.6 MBq/nmol) which were achieved using 3.5 nmol of DOTATATE precursor and a larger generator system (<222 MBq of ^{225}Ac) than available for this study (20 MBq of ^{225}Ac).[49] Serum stability measurements carried out on $[^{213}Bi][Bi(neunpa-Ph-Aoc-Pip-Nle-CycMSH_{hex})]$ showed no evidence of transmetalation to serum proteins over 2 h, further indicating a high degree of kinetic inertness (Figure S26).

LogD$_{7.4}$ Measurements. LogD$_{7.4}$ measurements determined for all four radiolabeled bioconjugates show a high degree of lipophilicity, with average values for the Aoc derivatives being higher than those without, as expected (Table 4).

Table 4. Radiochemistry Data for CycMSH$_{hex}$ Bioconjugates

compound	LogD$_{7.4}$	molar activity (MBq/nmol)
$[^{213}Bi][Bi(neunpa-Ph-Pip-Nle-CycMSH_{hex})]$	-1.683 ± 0.004[a]	21.0
$[^{213}Bi][Bi(neunpa-Ph-Aoc-Pip-Nle-CycMSH_{hex})]$	-1.103 ± 0.011[a]	7.47[c]
$[^{111}In][In(neunpa-Ph-Pip-Nle-CycMSH_{hex})]$	-0.838 ± 0.041[b]	1.30
$[^{111}In][In(neunpa-Ph-Aoc-Pip-Nle-CycMSH_{hex})]$	-0.759 ± 0.030[b]	316

[a]($n = 6$). [b]($n = 3$). [c]Determined using a low activity ^{225}Ac/^{213}Bi generator.

***In Vivo* Studies.** The high lipophilicity of the radiolabeled bioconjugates led to challenges for studying their *in vivo* performance, and as such, detailed procedures for the preparation of the $[^{213}Bi]Bi^{3+}$ and $[^{111}In]In^{3+}$ radiolabeled tracers are outlined in the Supporting Information. To maximize the injected dose per animal and minimize losses through surface adsorption, doses of each tested bioconjugate were prepared immediately prior to IV administration (<2 min delay).
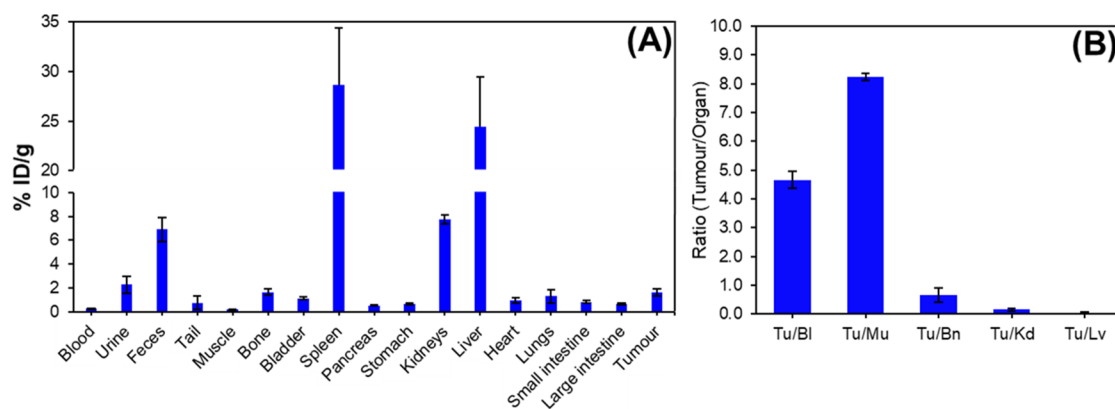
Biodistribution with $[^{213}Bi][Bi(neunpa-Ph-Pip-Nle-CycMSH_{hex})]$. Given the high molar activities accessible for $[^{213}Bi][Bi(neunpa-Ph-Pip-Nle-CycMSH_{hex})]$ (21.0 MBq/nmol) and more favorable LogD$_{7.4}$ value, it was decided to undertake biodistribution studies with $[^{213}Bi]Bi^{3+}$ using the bioconjugate without the additional Aoc spacer. Biodistribution studies of $[^{213}Bi][Bi(neunpa-Ph-Pip-Nle-CycMSH_{hex})]$ in C57B6/J mice bearing B16-F10 tumor xenografts showed moderate uptake in tumors at 1 h p.i. (5.91 ± 1.33%ID/g) with low uptake in nontarget organs (Figure 7). Typically, radiotracers exhibit an increased tumor uptake after 1 h post-administration; however, owing to the short half-life the mice were sacrificed and the tumors excised at this time-point. The radiolabeled bioconjugate exhibits fast clearance from blood circulation, as indicated by the low residual activity in the heart (1.22 ± 0.56%ID/g) and blood (1.35 ± 0.26%ID/g) and is excreted primarily via the renal pathway as evidenced by accumulation in the kidneys (44.19 ± 8.85%ID/g), and elimination in the urine. Notably, uptake in the liver (9.29 ± 1.24% ID/g) was observed at 1 h p.i., which is likely a consequence of the high lipophilicity of the $[^{213}Bi][Bi(neunpa-Ph-Pip-Nle-CycMSH_{hex})]$ tracer. The relatively low tumor uptake is to some extent a result of the presence of unlabeled precursor in the injected dose which gives rise to a partial blocking effect in the tumor. Mice were administered with doses consisting of ∼100 kBq of $[^{213}Bi]Bi^{3+}$ labeled with 20 pmol of H_4neunpa-Ph-Pip-Nle-CycMSH$_{hex}$, corresponding to a [L]:[M] of ∼30,000:1, a consequence of the available ^{225}Ac/^{213}Bi generator activity. As purification of the radiotracer from unlabeled precursor post-synthesis is not feasible for such a short-lived radionuclide, improvements to the molar activity, and thus tumor uptake, could be achieved by increasing the
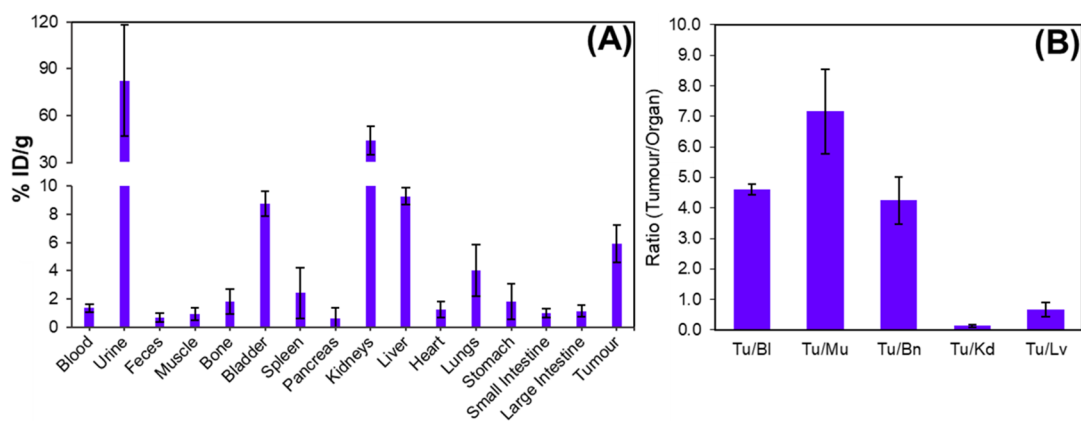
Figure 7. (A) Biodistribution data and (B) Tumor-to-organ ratios of $[^{213}Bi][Bi(neunpa-Ph-Pip-Nle-CycMSH_{hex})]$ in male C57bl/6J mice bearing B16-F10 melanoma tumor xenografts at 1 h p.i. ($n = 4$).
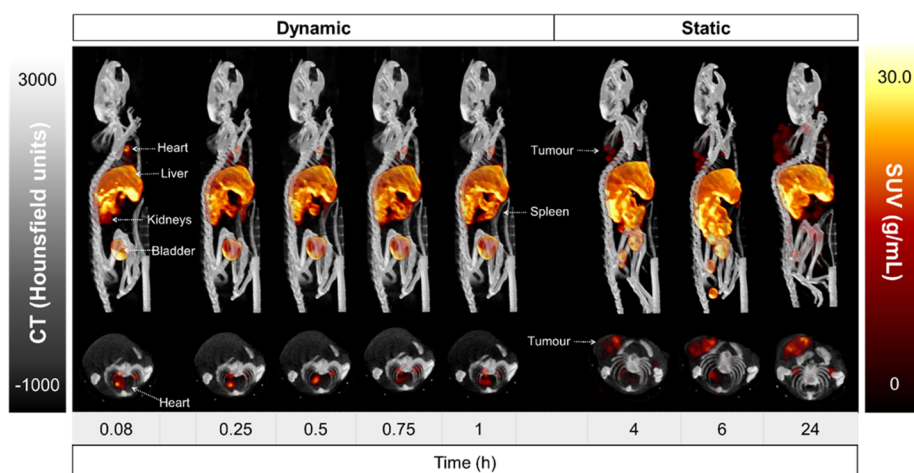
Figure 8. Sagittal (top) and transverse (bottom) views of maximum intensity projection (MIPs) on full-body SPECT/CT scans at 0−24 h after administration $[^{111}In][In(neunpa-Ph-Aoc-Pip-Nle-CycMSH_{hex})]$ (∼2.65 MBq) in male C57Bl/6J mice ($n = 3$) bearing B16-F10 tumor xenografts (right shoulder).

Figure 9. (A) Biodistribution profile and (B) Tumor-to-organ ratios of $[^{111}In][In(neunpa-Ph-Aoc-Pip-Nle-CycMSH_{hex})]$ in male C57Bl/6J mice bearing B16-F10 tumor xenografts at 24 h p.i.($n = 3$).

amount of $[^{213}Bi]Bi^{3+}$ used in each preparation, a viable strategy given the high molar activities achievable by $[^{213}Bi][Bi(neunpa-NH_3)]$.

***In Vivo* SPECT/CT with $[^{111}In][In(neunpa-Ph-Aoc-Pip-Nle-CycMSH_{hex})]$.** For the purpose of *in vivo* imaging in mice bearing B16-F10 tumor xenografts, the $[^{111}In][In(neunpa-Ph-Aoc-Pip-Nle-CycMSH_{hex})]$ radiotracer was selected for

SPECT/CT studies over the shorter linker analogue, given the high molar activities achievable (316 MBq/nmol); a prerequisite for effective targeting of B16-F10 melanomas. Quantitative dynamic SPECT/CT images of mice bearing B16-F10 tumor xenografts were acquired over a period of 24 h to assess the biodistribution and pharmacokinetics of $[^{111}In]$-$[In(neunpa-Ph-Aoc-Pip-Nle-CycMSH_{hex})]$ after intravenous

administration (Figure 8). Quantified uptake values in multiple organs of interest (heart, bladder, kidneys, liver, and tumor) were expressed as mean standardized uptake values (SUVs) versus time to generate time−activity curves for regions of interest (ROIs), Figure S28.

Sagittal and transverse views show rapid clearance of the radiotracer from blood circulation over the first hour after administration and further excretion through the urinary tract, as evidenced through activity in the kidneys, bladder, and urine, whereby ∼30% of the total injected activity (%IA) is excreted after 4 h. Besides the renal clearance, a predominant elimination through the hepatic pathway, leading to an increased concentration in the liver (SUV_{mean} = 9.68 ± 1.66 g/mL) and spleen (SUV_{mean} = 7.55 ± 2.14 g/mL), is also observed within the first 5 min after administration of $[^{111}In][In(neunpa-Ph-Aoc-Pip-Nle-CycMSH_{hex})]$. The radiotracer is retained and cleared slowly after 24 h (liver SUV_{mean} = 7.29 ± 0.84 g/mL) through the bile and intestinal tract, followed by elimination in the feces after 24 h p.i.

Tumor uptake is clearly visualized in the transverse projections beginning at 4 h p.i. Assessment of the organ-specific time−activity curves show that uptake in the tumor is correlated with clearance from the blood circulation, as expected, wherein maximum SUVs were achieved after 24 h p.i. (Figure S28). Ex vivo biodistribution studies performed after acquisition of the final SPECT/CT scans determined an average tumor uptake of 1.64 ± 0.30%ID/g (n = 3) (Figure 9). The low tumor uptake determined for $[^{111}In][In(neunpa-Ph-Aoc-Pip-Nle-CycMSH_{hex})]$ was primarily a consequence of the high lipophilicity which led to rapid accumulation and retention in the liver within the first 5 min after administration. The high lipophilicity is further reflected in the tumor-to-organ ratios at 24 p.i. (Figure 9B), wherein tumor-to-liver and tumor-to-kidney ratios of 0.04 and 0.15, respectively, highlight the strong retention of the radiotracer in these organs, while tumor-to-blood and tumor-to-muscle ratios peak at 4.66 and 8.23, respectively.

Accumulation of radioactivity in the bone marrow (1.92 ± 0.26%ID/g) is seen at 24 h p.i.; however, this observation was not attributed to poor metal-chelate stability, since free $[^{111}In]In^{3+}$ is rapidly bound by serum proteins and localized in the liver and lungs. Furthermore, previous studies of $[^{111}In][In(neunpa-Bn-NO_2)]$ and $[^{111}In][In(neunpa-trastuzumab)]$ showed excellent in vivo stability up to 5 days post-administration with minimal bone accumulation;[37] therefore, we concluded that in the case of $[^{111}In][In(neunpa-Ph-Aoc-Pip-Nle-CycMSH_{hex})]$ metabolic degradation in the liver as a result of the fast initial accumulation and retention (31.5 ± 4.99%ID/g) may be responsible for the bone accumulation at later time-points, in addition to possible uptake of the radiotracer by macrophages and subsequent transportation to bone marrow.

As noted above, the $LogD_{7.4}$ values determined for all four radiotracers were considerably more lipophilic than those previously reported for $[^{68}Ga]Ga-CCZ01048$ ($LogD_{7.4}$ = −3.14 ± 0.04) which incorporates the same targeting vector and piperidine spacer, with DOTA as the chelating ligand.[21] Furthermore, prior in vivo studies of similar picolinate-based bifunctional chelators and their corresponding peptide-bioconjugates have been shown to be fairly hydrophilic, giving good in vivo performance, with low nontarget organ accumulation.[50] In the case of the bioconjugates reported here, it was the selection of the p-phenylene bis-thiourea

conjugation handle, and further combination with the Aoc linker which ultimately dictated the high lipophilicity and subsequent poor in vivo performance, rather than the inherent properties of the ligand or peptide. Incorporation of a more hydrophilic covalent linker (e.g., PEG) by direct conjugation to the free primary amine of $H_4neunpa-NH_2$ would be expected to give a significant improvement to the biological effectiveness of this radiotracer.

CONCLUSIONS

This study reports $H_4neunpa-NH_2$ as a bifunctional chelating ligand in combination with $[^{111}In]In^{3+}$ and $[^{213}Bi]Bi^{3+}$ for theranostics in PRRT. X-ray crystallographic studies of the metal complexation with $[^{nat}Bi]Bi^{3+}$ show that the binding cavity of $H_4neunpa-NH_2$ is ideally matched to the ionic radius of the metal ion, forming a single, asymmetric isomer with all nine donor atoms bound. Evaluation of the radiolabeling properties with $[^{111}In]In^{3+}$ and $[^{213}Bi]Bi^{3+}$ demonstrated highly effective coordination, achieving quantitative RCYs within 5 min at RT at ligand concentrations of 10^{-7} and 10^{-8} M, respectively, which was accompanied by the formation of kinetically inert complexes. These promising characteristics warranted the development of a suitable bioconjugate incorporating $H_4neunpa-NH_2$ and cyclic-αMSH derivative for the assessment of potential in vivo application in targeting MC1R in cutaneous melanomas. High molar activities of 21 MBq/nmol were achieved for $[^{213}Bi][Bi(neunpa-Ph-Pip-Nle-CycMSH_{hex})]$, and evaluation of the in vivo biodistribution profile in tumor bearing mice showed promising initial results, with moderate tumor uptake (5.91 ± 1.33%ID/g) at 1 h p.i. Further development of the bioconjugate through incorporation of an 8-aminooctanyl (Aoc) linker gave notable improvements in radiolabeling efficiencies with both $[^{111}In]-In^{3+}$ and $[^{213}Bi]Bi^{3+}$. SPECT/CT and biodistribution studies with $[^{111}In][In(neunpa-Ph-Aoc-Pip-Nle-CycMSH_{hex})]$ showed unintended pharmacokinetic properties, with high liver uptake within 5 min post-administration and high organ retention (31.5 ± 4.99%ID/g liver), ultimately dictated by the high lipophilicity of $[^{111}In]In^{3+}$—labeled tracer—a consequence of the covalent linker and bioconjugation approach selected. These studies demonstrate $H_4neunpa-NH_2$ to be a versatile and effective chelating ligand for both In^{3+} and Bi^{3+}, with encouraging characteristics for the application of $[^{111}In]In^{3+}$ and $[^{213}Bi]Bi^{3+}$ as a theranostic pair, when combined with appropriate biological targeting vectors. Further developments of the existing bioconjugates to incorporate more hydrophilic covalent linkers should give significant improvements to the in vivo performance and the ease of radiotracer preparation. The ligand $H_4neunpa-NH_2$ and related constructs suggest great possibilities for radio-applications.

EXPERIMENTAL SECTION

Methods and Materials. All solvents and reagents were purchased from commercial suppliers (Sigma-Aldrich, AK Scientific, Alfa Aesar) and were used directly without further purification. Analytical thin-layer chromatography (TLC) sheets were purchased from Merck (TLC Silica gel 60 F254, aluminum sheet). Deionized H_2O (18.2 MΩ/cm at 25 °C) was obtained from a PURELAB Ultra water purification system, ELGA LabWater. Flash column chromatography was performed using Siliaflash F60 silica gel (60 Å, 40−63 μm particle size, 230−400 mesh) from Silicycle Inc. Automated

column chromatography was performed using a Teledyne Isco (Lincoln, NE) CombiFlash Rf automated purification system equipped with RediSep Rf Gold HP prepacked reusable silica and neutral alumina column cartridges. Low-resolution mass spectrometry (LR-MS) was performed using a Waters 2965 ZQ spectrometer with an electrospray/chemical ionization (ESI/CI) source. High-resolution mass spectrometry (HR-MS) was performed using a Waters Micromass LCT TOF instrument. Elemental analyses (CHN) were carried out using a Thermoflash 2000 elemental analyzer. ^{1}H and ^{13}C{^{1}H} NMR spectra were recorded using Bruker AV300 and AV400 spectrometers; all spectra are reported on the delta scale referenced to residual solvent peaks. Analytical and semi-preparative high-performance liquid chromatography (HPLC) was carried out using a Waters 600 system equipped with a Waters 2487 dual wavelength absorbance detector monitoring at 254 and 210 nm and a Phenomenex Synergi 250 mm × 21.2 mm 4 μm hydro-RP80 Å column (10 mL/min). All HPLC methods employed a H$_2$O/MeCN biphasic solvent system buffered with 0.1% TFA. [^{111}In]InCl$_3$ ($t_{1/2}$ = 2.83 days) (purchased from BWX Technologies) was produced by proton irradiation (Advanced Cyclotron Systems, Model TR30) via the^{111}Cd(p,n)^{111}In reaction and provided as a 0.05 M HCl solution. [^{225}Ac]Ac(NO$_3$)$_3$ ($t_{1/2}$ = 10.0 days) was produced at TRIUMF via the spallation of ^{232}Th targets with 500 MeV protons and purified as previously reported.[51] [^{213}Bi][BiI$_5$]$^{2-}$ was obtained from an in-house ^{225}Ac/^{213}Bi generator constructed using AG-MP-50 cation exchange resin, based on established methodologies.[47] Radiolabeling of compounds was assessed via instant thin-layer chromatography (iTLC) using silicic acid (SA)-impregnated paper TLC plates sourced from Agilent technologies. TLC imaging was performed using an AR-2000 imaging scanner equipped with PD-10 gas, and subsequent analysis of radiochemical conversion (RCC) was carried out using WinScan V3_14 software. Radio-HPLC was carried out using an Agilent 1200 instrument equipped with a Phenomenex Synergi 4 μm 250 mm × 4.6 mm hydro-RP 80 Å column. Quantification of [^{111}In]In^{3+} radioactivity was achieved using a Capintec CRC-15R dose calibrator (Capintec, Ramsey, NJ). [^{213}Bi]Bi^{3+} radioactivity was quantified using a high-purity germanium (HPGe) detector (Mirion Technologies (Canberra)Inc.) with Genie 2000 software using the γ emission lines from ^{213}Bi ($t_{1/2}$= 45.6 min, 440 keV, 25.9% abundance) and ^{209}Tl (2.2 min, 465 keV, 96.9% abundance). All work with radionuclides at TRIUMF was undertaken in shielded fume hoods to minimize dose to experimenters (and special precautions were used to prevent contamination) under nuclear energy worker (NEW) status earned by attending TRIUMF's Advanced Radiation Protection course and passing the final exam. Cyclic-αMSH peptides were prepared by the BCCA using similar approaches to previously published procedures.[21] SPECT/CT studies were performed using a multimodal VECTor/CT system (MILabs, Netherlands) in combination with an extra ultrahigh-sensitivity (XUHS) 2 mm pinhole collimator. Image analysis was performed using AMIDE (v 1.0.4) software.

Synthesis.
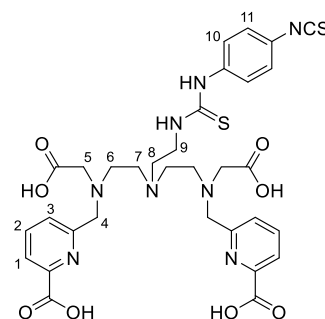
H$_4$neunpa-Ph-NCS (2). H$_4$neunpa-NH$_2$·6HCl (prepared as previously described[38]) (21.0 mg, 26.6 μmol) was suspended in anhydrous DMF (700 μL) and basified with Na$_2$CO$_3$ (29 mg, 266 μmol, 10 equiv). The suspension was stirred vigorously for 10 min at RT before addition of p-phenylene diisothiocyanate (51 mg, 266 μmol). The resulting mixture was stirred overnight, protected from light. Upon completion, the pale-yellow suspension was separated via centrifuge and the insoluble salts washed with DMF (2 × 1 mL). The combined supernatant was divided between two centrifuge tubes and diluted with diethyl ether (2 × 10 mL). The product precipitated on standing at 5 °C for 1 h, isolated via centrifuge and washed with diethyl ether (2 × 10 mL). The crude material was purified via semipreparative RP-HPLC (A: H$_2$O (0.1% TFA), B: MeCN; 95% A to 50% B, 45 min gradient, 10 mL/min., t_R = 35.2 min.). Appropriate product fractions were pooled and lyophilized to give the title compound as a white solid (15.7 mg, 78%). ^{1}H NMR (400 MHz, D$_2$O, d_3-MeCN, 298 K) 8.30 (2H, t, ^3J = 7.7 Hz, 2 − CH), 8.20 (2H, d, ^3J = 7.7 Hz, 1 − CH), 7.85 (2H, d, ^3J = 7.7 Hz, 3 − CH), 7.21 (2H, d, ^3J = 8.4 Hz, 11 − CH), 7.13 (2H, d, ^3J = 8.4 Hz, 10 − CH), 4.38 (4H, s, 4 − CH_2), 4.16 (2H, br t, ^3J = 5.0 Hz, 9 − CH_2), 3.83 (4H, s, 5 − CH_2), 3.66−3.61 (6H, m, 6−and 8 − CH_2), 3.43 (2H, t, ^3J = 6.1 Hz). ESI-MS (H$_2$O) 725.3 [M + H]$^+$, 363.3 [M+2H]$^{2+}$.
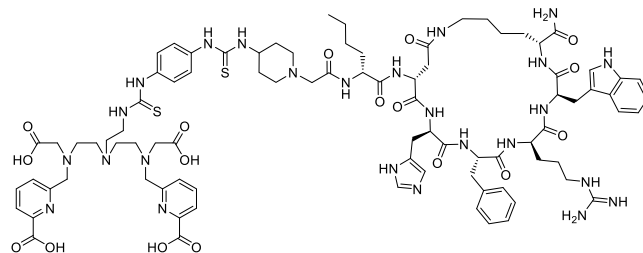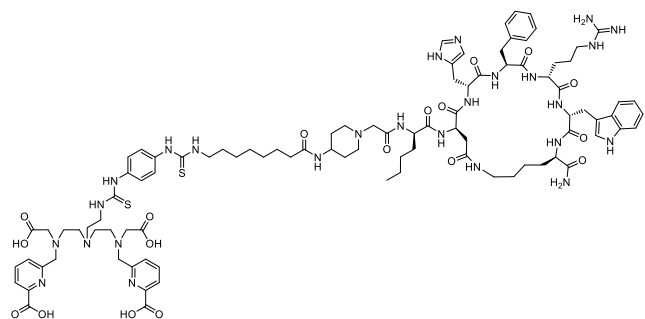

H$_4$neunpa-Ph-Pip-Nle-CycMSH$_{hex}$ (3). H$_4$neunpa-Ph-NCS (6.9 mg, 9.6 μmol) and Pip-Nle-CycMSH$_{hex}$ peptide (prepared as previously described[21]) (10.6 mg, 9.5 μmol) were dissolved in anhydrous DMF (500 μL) and the yellow solution basified with Na$_2$CO$_3$ (10.8 mg, 94 μmol). The reaction mixture was stirred vigorously overnight at RT. Upon completion, the suspension was transferred to a centrifuge tube, and the insoluble salts separated. The salts were washed with DMF (3 × 500 μL) and the combined supernatant distributed between two centrifuge tubes. The crude bioconjugate was precipitated in diethyl ether and purified via semipreparative RP-HPLC (A: H$_2$O (0.1% TFA), B: MeCN; 95% A to 45% B, 50 min gradient, 10 mL/min., t_R = 41.0 min.). ESI-MS (H$_2$O/MeCN) 1846.8 [M + H]$^+$, 923.5 [M+2H]$^{2+}$, 616.7 [M+3H]$^{3+}$, 1844.8 [M-H]$^-$, 921.4 [M-2H]$^-$. HR-ESI-MS (H$_2$O/MeCN) calcd. for [C$_{87}$H$_{115}$N$_{25}$O$_{17}$S$_2$ + H]$^+$: 1846.8350; found [M + H]$^+$: 1846.8427.
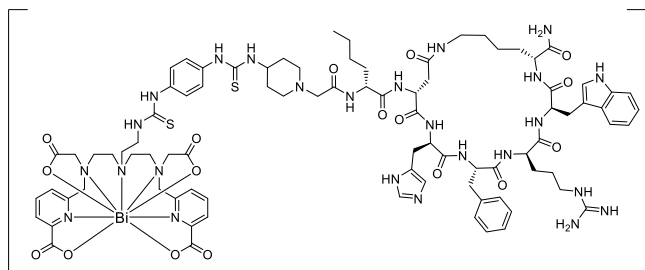
[^{nat}Bi][Bi(neunpa-Ph-Pip-Nle-CycMSH$_{hex}$)] *(4).* Bi(NO$_3$)$_3$·5H$_2$O (1.5 mg, 3.09 μmol) was added to a solution of H$_4$neunpa-Pip-Nle-CycMSH$_{hex}$ (5.0 mg, 2.71 μmol) in deionized H$_2$O (500 μL) and the pH adjusted to 5.0 with 1 M NaOH solution. The reaction mixture was allowed to stir for 30 min at RT, after which time the corresponding Bi^{3+}-peptide conjugate was purified via semipreparative HPLC (A: H$_2$O (0.1% TFA), B: MeCN; 95% A to 45% B, 50 min gradient, 10 mL/min, t_R = 38.0 min.). Appropriate fractions were combined and lyophilized to attain the product as a white solid. ESI-MS (H$_2$O/MeCN) 2052.8 [M + H]$^+$, 1026.5 [M +2H]$^{2+}$. HR-ESI-MS (H$_2$O/MeCN) calcd. for [C$_{87}$H$_{112}$BiN$_{25}$O$_{17}$S$_2$ + H]$^+$: 2052.7913; found [M + H]$^+$: 2052.7978.

H$_4$neunpa-Ph-Aoc-Pip-Nle-CycMSH$_{hex}$ *(5).* H$_4$neunpa-Ph-NCS (3.1 mg, 4.1 μmol) and H$_2$N-Aoc-Pip-Nle-CycMSH$_{hex}$ (kindly provided by Department of Molecular Oncology, BC Cancer Agency, Vancouver, BC, Canada) (5.2 mg, 4.1 μmol) were dissolved in anhydrous DMF (250 μL) and the yellow solution basified with DIPEA (8 μL, 46 μmol). The reaction mixture was stirred vigorously overnight at RT. Upon completion, the solution was transferred to a centrifuge tube, and the crude bioconjugate precipitated in diethyl ether (10 mL). After cooling for 1 h at 0 °C, the white precipitate was separated by centrifuge and purified via semipreparative RP-HPLC (A: H$_2$O (0.1% TFA), B: MeCN; 95% A to 50% B, 45 min gradient, 10 mL/min, t_R = 27.0 min.). LR-ESI-MS (H$_2$O/MeCN) 1987.8 [M + H]$^+$, 994.05 [M+2H]$^{2+}$, 663.7 [M +3H]$^{3+}$, 1985.8 [M-H]$^-$, 992.2 [M-2H]$^-$. HR-ESI-MS (H$_2$O/MeCN) calcd. for [C$_{95}$H$_{130}$N$_{26}$O$_{18}$S$_2$ + H]$^+$: 1987.9501; found [M + H]$^+$: 1987.9573.
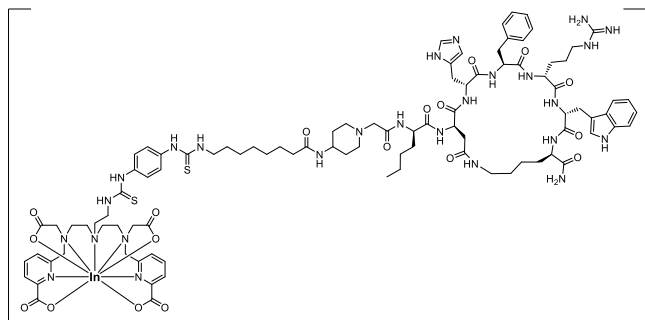
[^{nat}In][In(neunpa-Ph-Aoc-Pip-Nle-CycMSH$_{hex}$)](6). An aqueous solution of In(NO$_3$)$_3$·H$_2$O (100 μL, 3.55 mg/mL, 1.1 μmol) was added to H$_4$neunpa-Ph-Aoc-Pip-Nle-CycMSH$_{hex}$ (2.0 mg, 1.1 μmol) dissolved in MeCN/H$_2$O (1:1) (200 μL) and the pH adjusted to ~5 with NaOH (0.1 M, 50 μL). The turbid mixture was stirred for 2 h, and then diluted with deionized H$_2$O (0.1% TFA) and purified via semipreparative RP-HPLC (A: H$_2$O (0.1% TFA), B: MeCN; 95% A to 50% B, 45 min gradient, 10 mL/min., t_R= 29.3 min.). LR-ESI-MS (H$_2$O/MeCN) 2099.6 [M+2H]$^+$, 1050.6 [M+3H]$^{2+}$, 700.3 [M+4H]$^{3+}$, 2097.6 [M]$^-$. HR-ESI-MS (H$_2$O/MeCN) calcd. for [C$_{95}$H$_{126}$InN$_{26}$O$_{18}$S$_2$ + 2H]$^+$: 2099.8331; found [M +2H]$^+$: 2099.8392, [M+3H]$^{2+}$: 1050.4250.
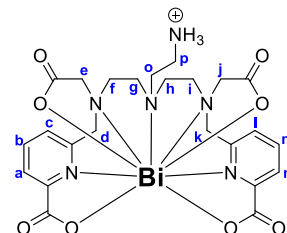
[^{nat}Bi][Bi(neunpa-NH$_3$)]). Bi(NO$_3$)$_3$·5H$_2$O (6.5 mg, 13.3 μmol) was added to a solution of H$_4$neunpa-NH$_2$ · 6HCl (prepared as previously described[38]) (10 mg, 13.3 μmol) in deionized H$_2$O (300 μL) and the pH adjusted to ~5 using NaOH solution (1 M). The turbid mixture was stirred at RT for 1 h, then filtered through a 0.2 μm cellulose membrane and lyophilized to give a white powder. The isolated material was redissolved in D$_2$O (400 μL) and analyzed directly by NMR spectroscopy and LR/HR-ESI-MS. ^{1}H NMR (400 MHz, D$_2$O, 298 K, pD 7) 8.28 (1H, t, ^3J = 8.0 Hz, b − CH), 8.11 (1H, t, ^3J = 7.8 Hz, m − CH), 8.02 (1H, d, ^3J = 8.0 Hz, a − CH), 7.92−7.90 (2H, m, c− and n − CH), 7.75 (1H, d, ^3J = 7.8 Hz, l − CH), 4.76 (2H, br m, d' − and k' − CH$_2$), 4.51 (1H, d, ^2J = 14.8 Hz, d'' − CH$_2$), 4.47 (1H, d, ^2J = 16.8 Hz, k'' − CH$_2$), 4.01 (1H, d, ^2J = 16.5 Hz, e' − CH$_2$), 3.97 (1H, d, ^2J = 17.3 Hz, j' − CH$_2$), 3.84 (1H, d, ^2J = 16.5 Hz, e'' − CH$_2$), 3.73 (1H, app d, f' − CH$_2$), 3.62 (1H, app d, i' − CH$_2$), 3.46 (1H, d, ^2J = 17.3 Hz, j'' − CH$_2$), 3.44 (1H, m, o' − CH$_2$), 3.31 (1H, app d, o'' − CH$_2$), 3.11−3.02 (3H, m, i'' − , p' and h' − CH$_2$), 2.85−2.74 (2H, m, g' − and h'' − CH$_2$), 2.65−2.62 (2H, m, f'' − and p'' − CH$_2$), 2.39 (1H, m, g'' − CH$_2$). LR-ESI-MS (H$_2$O) 739.0 [M + H]$^+$, 761.0 [M + Na]$^+$, 772.7 [M+Cl]$^-$. HR-ESI-MS (H$_2$O) calcd. for [C$_{24}$H$_{29}$BiN$_6$O$_8$ + H]$^+$: 739.1852; found [M + H]$^+$: 739.1926.

DFT Calculations. Density functional theory (DFT) calculations were carried out using the Gaussian 16 (revision B.01) software package.[52] Geometry optimizations were performed using the M06-2X functional, a meta-hybrid generalized gradient approximation (GGA) functional with empirical dispersion inclusion which has shown good performance in modeling of main group coordination complexes.[43−45] Large-core fully relativistic effective core potentials (ECP78MDF) and the related (6s6p3d2f)/[4s4p3d2f] valence basis set were used for modeling of Bi^{3+},[53] while the Def2TZVP basis set was used for lighter atoms (C, N, H, O). Initial molecular mechanics optimized structures were generated in Avogadro (v 1.2.0)[54] and used as input coordinates for DFT geometry optimizations. All geometry optimizations were modeled in aqueous solution using the integrated equation formalism polarizability continuum model (IEF-PCM) incorporated in Gaussian 16. Vibrational

frequency calculations were performed to determine whether final optimized structures were true energy minima on the potential energy surface. Full natural bond orbital (NBO) analysis was performed using NBO (version 3.1)[55] incorporated within Gaussian 16.

X-ray Crystallography (CCDC #2141221). A colorless prism-shaped crystal with dimensions $0.09 \times 0.06 \times 0.04$ mm^3 was mounted on a MITIGEN holder in oil. Data were collected using a Bruker APEX II area detector diffractometer equipped with a Kryoflex low-temperature device operating at $T = 140(2)$ K. Data were measured using ϕ and ω scans of $0.5°$ per frame for 60 s using MoK$_\alpha$ radiation (microfocus sealed X-ray tube, 50 kV, 0.99 mA). The total number of runs and images was based on the strategy calculation from the program APEX3. The maximum resolution that was achieved was $\Theta = 26.424°$ (0.80 Å). The unit cell was refined using SAINT (Bruker, V8.40B, after 2013) on 4404 reflections, 84% of the observed reflections. Data reduction, scaling, and absorption corrections were performed using SAINT (Bruker, V8.40B, after 2013).[56] The final completeness is 100.00% out to $26.424°$ in Θ. The material was integrated as a two-component nonmerohedral twin. Final HKLF 4 output contains 53077 reflections, $R_{int} = 0.1343$ (24709 with $I > 3\text{sig}(I)$, $R_{int} = 0.1093$). The absorption coefficient μ of this material is 6.692 mm^{-1} at this wavelength ($\lambda = 0.71073$ Å) and the minimum and maximum transmissions are 0.399 and 0.765. The structure was solved and the space group $Pna2_1$ (# 33) determined by the XT structure solution program using Intrinsic Phasing methods and refined by full matrix least-squares minimization on F^2 using version 2018/3 of XL.[57] All non-hydrogen atoms were refined anisotropically. Hydrogen atom positions were calculated geometrically and refined using the riding model. Olex2 was used as the graphical interface for structural refinements.[58]

Cell Culture and Receptor Binding Assays. B16F10 tumor cells, a MC1R-postive murine melanoma cell line from C57Bl/6J mice, were cultured as previously reported by Zhang et al.[21] In vitro competitive binding assays were performed in the B16F10 cell line using an analogous approach to previously reported methods.[21] The nonradioactive In^{3+} and Bi^{3+}-labeled αMSH bioconjugates and ^{125}I-[Nle^4, D-Phe^7]-α-MSH (PerkinElmer) were added to 24 well plates seeded with B16F10 cells. Competitive binding of ^{125}I-[Nle^4, D-Phe^7]-α-MSH to MC1R was performed using increasing concentrations of each ligand over a concentration of 0.5 pM to 5 μM. Plates were incubated at 25 °C with gentle agitation for 1 h, after which the media were removed, and the cells washed with cold PBS (2×) and harvested by addition of Trypsin. Radioactivity was measured using a WIZARD 2480 gamma counter (PerkinElmer) to determine receptor binding affinity.

Radiochemistry. ^{225}Ac/^{213}Bi Generator System. A large-scale ^{225}Ac/^{213}Bi generator ($\sim$25 MBq) was constructed using established methodologies based on AGMP-50 cation exchange separation technique.[48] AGMP-50 cation exchange resin (70 mg) was packed into a 1 mL reservoir, equipped with polyethylene frits, and pre-equilibrated with 4 M HNO$_3$ (2 mL). ^{225}Ac (25 MBq) dissolved in 4 M HNO$_3$ (4 mL) was batch loaded into the column, and the resin washed with a further aliquot of 4 M HNO$_3$ (2 mL). ^{213}Bi was eluted from the ^{225}Ac/^{213}Bi generator using freshly prepared 0.1 M NaI/0.1 M HCl solution (600 μL), wherein the bulk of the ^{213}Bi activity was eluted in the first 150 μL.

Radiolabeling with [^{213}Bi]Bi^{3+}. Stock solutions of chelates and bioconjugates (1×10^{-3} M) were prepared in ultrapure deionized H$_2$O and subsequent dilution series ($10^{-4} - 10^{-8}$ M) prepared for use in further labeling reactions. Concentration-dependent radiolabeling studies were performed by addition of [^{213}Bi][BiI$_4$]$^-$/[^{213}Bi][BiI$_5$]$^{2-}$ (10 μL, $\sim$650 kBq) to solutions containing ligand stock (10 μL) in MES buffer (30 μL, 1 M, pH 5.5). All radiolabeling studies were carried within 5 min post-elution of the ^{225}Ac/^{213}Bi generator. Each labeling reaction was allowed to stand at RT for 5−10 min, and the radiochemical conversion (RCC) determined via iTLC using silicic acid impregnated paper TLC plates with EDTA (50 mM, pH 5.5) as eluent. Under these conditions, free ^{213}Bi migrates with the solvent front ($R_f = 1$) while the chelated species remain at the baseline ($R_f = 0$). RCCs were confirmed by analysis of the baseline and solvent front TLC peaks using a high-purity germanium (HPGe) detector and monitoring the 440 keV γ emission line of ^{213}Bi. In all studies carried out, control reactions were performed in parallel by addition of [^{213}Bi]Bi^{3+} (10 μL, 650 kBq) to solutions containing MES buffer (30 μL, 1 M, pH 5.5) and deionized H$_2$O (10 μL). Representative iTLC plates are provided in Figure S19.

Radiolabeling with [^{111}In]In^{3+}. Concentration-dependent radiolabeling studies were carried out by addition of [^{111}In]-InCl$_3$ (1−2 μL, 1.0−1.3 MBq) to solutions containing H$_4$neunpa-NH$_3$, H$_4$neunpa-αMSH, or H$_4$neunpa-Aoc-αMSH (10 μL, 10^{-3} to 10^{-8} M) in NH$_4$OAc buffer (90 μL, 0.5 M, pH 5.5). Radiolabeling reactions were carried at RT and reaction progress monitored by iTLC using SA-paper TLC plates with EDTA (50 mM, pH 7) as eluent. Separate control reactions were carried out by addition of [^{111}In]InCl$_3$ (1 MBq) to NH$_4$OAc buffer (100 μL, 0.5 M, pH 5.5) and monitored under the same conditions assessed for each ligand. Representative iTLC plates are provided in the Supporting Information, Figure S20.

[^{111}In]In^{3+} Radiotracer Preparation. H$_4$neunpa-Ph-Aoc-Pip-Nle-CycMSH$_{hex}$ (1 nmol, 10 μL, 10^{-4} M) was radiolabeled with [^{111}In]InCl$_3$ (316 MBq, 40 μL, 0.05 M HCl) in NH$_4$OAc buffer (0.5 M, 20 μL, pH 5.5) and MeCN (20 μL) at RT. The reaction solution was allowed to stand for 15 min at RT and quantitative RCC confirmed via iTLC using SA-paper plates and EDTA (50 mM, pH 5.5) as eluent. The radiolabeling solution was diluted with deionized H$_2$O (0.1% TFA)/MeCN (2:1) (130 μL) and injected on to a semipreparative HPLC system. [^{111}In][In(neunpa-Ph-Aoc-Pip-Nle-CycMSH$_{hex}$)] was separated from unlabeled precursor using an isocratic HPLC method (70% H$_2$O (0.1% TFA), 30% MeCN (0.1% TFA); flow rate: 1 mL/min) whereby the radiolabeled product elutes with retention time of $T_R = 26.45$ min, while unlabeled precursor elutes with a retention time of $T_R = 24.83$ min. Collected fractions containing purified [^{111}In][In(neunpa-Ph-Aoc-Pip-Nle-CycMSH$_{hex}$)] ($\sim$2 mL) were pooled and diluted with deionized H$_2$O (4 mL) to give a solution suitable for Sep-Pak purification (<10% MeCN v/v). The diluted stock solution was batch-loaded on a Sep-Pak C18 Plus Light cartridge (Waters) previously equilibrated with EtOH (4 mL), then deionized H$_2$O (10 mL). The loaded cartridge was washed with deionized H$_2$O (1 mL) and eluted with EtOH/ 0.9% NaCl saline (9:1, 1 mL). The elution fraction was reduced in volume ($\sim$100 μL) by passage of N$_2$ gas over 30 min, and the final product was reconstituted in PBS/EtOH solution (9:1, pH 7.4; $V_T = 525$ μL). Quality control was

performed using radio-HPLC and iTLC; isolated product of >95% radiochemical purity was used for further studies.

$[^{213}Bi]Bi^{3+}$ *Radiotracer Preparation.* Freshly eluted $[^{213}Bi]$-Bi^{3+} (1.95 MBq, 30 μL) was added to a solution containing H_4neunpa-Ph-Pip-Nle-CycMSH$_{hex}$ (200 pmol, 2 μL, 10^{-4} M), MES buffer (1.0 M, 20 μL, pH 5.5), and NaOH (1 M, 6 μL). The reaction mixture was agitated for 5 min at RT, and then diluted with a solution of L-ascorbate (250 mM) in 0.9% NaCl saline/EtOH (9:1; 942 μL). Quality control was performed via iTLC measurements to confirm >95% radiochemical purity. An aliquot of $[^{213}Bi][Bi($neunpa-Ph-Pip-Nle-CycMSH$_{hex})]$ (100 μL, 20 pmol) was taken for dose determination using γ spectroscopy prior to *in vivo* studies. Final molar activity of 4.7 MBq/nmol was achieved at the end of radiochemical synthesis.

LogD$_{7.4}$ Measurements. Aliquots of each radiolabeled bioconjugate (10 μL) were added to a biphasic mixture of *n*-octanol (700 μL) and PBS (700 μL, pH 7.4). The mixture was vortexed for 2 min at RT and then separated via centrifuge (10 min, 3000 rpm). Aliquots of *n*-octanol (100 μL) and PBS (100 μL) were collected, and the activity in each portion determined via γ spectroscopy. The LogD$_{7.4}$ is defined as $\log_{10}[(n\text{-octanol phase})/(\text{buffer phase})]$.

Biodistribution Studies. *Tumor Implantation.* The tumor implantation was performed the under the protocol approved by the Animal Care Committee (ACC) of the University of British Columbia (A20−0113). Male C57bl/6J mice were anesthetized by inhalation with 2% isoflurane in 2.0 L/min of oxygen, and 2×10^6 B16-F10 cells were implanted subcutaneously on the right back at the level of the forelimbs. *In vivo* imaging and biodistribution studies were performed after tumor growth reached a diameter of ~8−10 mm (8−10 days post-implantation).

Preclinical SPECT/CT. Animal studies were performed in accordance with the Canadian Council on Animal Care (CCAC) using the protocol approved by the Animal Care Committee (ACC) of the University of British Columbia (A20−0132). Three C57bl/6J male mice bearing B16-F10 tumor xenografts were anesthetized with 5% isoflurane in an induction chamber and restrained in a Tail vein Restrainer (Braintree Scientific) while under a continuous stream of 1−1.5% isoflurane. Mice were administered with $[^{111}In][In$-(neunpa-Ph-Aoc-Pip-Nle-CycMSH$_{hex})]$ (~2.65 MBq) in PBS (150 μL) via lateral tail vein. Animal subjects were maintained at constant body temperature using a blanket on a heated bed, maintained under continuous stream of 1.5−2% isoflurane, and the respiration rate monitored throughout the duration of each scan. Immediately after injection, whole-body dynamic SPECT/CT scans were acquired over the first 60 min using a multimodal VECTor/CT system (MILabs, Netherlands) equipped with an extra ultrahigh-sensitivity (XUHS) 2 mm pinhole collimator. The mouse whole-body region was centered with a 14 mm axial field of view, and dynamic imaging consisting of five frames of 10 min were acquired over the first 60 min, after which static SPECT/CT scans were recorded at 4, 6, and 24 h post-injection using single frames of 20 and 30 min acquisitions. An energy window centered on the 171 keV photopeak of ^{111}In was used, with a spectral width of 25%. To permit quantitation, the SPECT images were reconstructed using pixel-based ordered-subset expectation maximization (POSEM) reconstruction algorithm using a voxel size of 0.4 mm^3, 16 subsets with 6 iterations. SPECT images were decay-corrected and attenuation factors applied based on CT acquisitions at each time-point.[59] A calibration

factor relating (counts/voxel) to radioactivity concentration was previously determined by measurement of a known source of ^{111}In. Spherical volumes of interest (VOIs) (3 mm diameter) were drawn using AMIDE (v 1.0.4) software to determine the pharmacokinetic profile of the tracer in target organs of interest. Average standardized uptake values (SUVs) were subsequently extracted from the SPECT images. Gaussian filtering and image rendering was carried post-reconstruction for data visualization purposes. The standardized uptake value was defined according to the equation: SUV (g/mL) = radioactivity concentration (MBq/mL)/ [administered dose (MBq)/body weight (g)].

$[^{111}In][In($neunpa-Ph-Aoc-Pip-Nle-CycMSH$_{hex})]$. After acquisition of the final SPECT/CT scan at 24 h post-injection, mice were sacrificed via CO_2 asphyxiation under 2% isoflurane anesthesia, followed by cardiac puncture to remove blood. Organs of interest were harvested and weighed prior to measurement of radioactivity using a calibrated gamma counter (Packard Cobra II Autogamma counter, PerkinElmer, Waltham, MA, USA) with a 1 min acquisition time per sample. All radioactivity measurements were decay corrected to the time of injection, and the injected dose per gram of tissue (%ID/g) calculated based on measured organ weights, with the exception of blood, bone, and muscle which were scaled in accordance with literature values.[60]

$[^{213}Bi][Bi($neunpa-Ph-Pip-Nle-CycMSH$_{hex})]$. Biodistribution studies with $[^{213}Bi][Bi($neunpa-Ph-Pip-Nle-CycMSH$_{hex})]$ were performed in four male C57bl/6J mice bearing B16-F10 tumors. Mice were anaesthetized by 2% isoflurane inhalation and restrained in a tail vein restrainer (Braintree Scientific) prior to injection with $[^{213}Bi][Bi($neunpa-Ph-Pip-Nle-CycMSH$_{hex})]$ (~100 kBq) in PBS (~100 μL) via lateral tail vein. After injection, mice were allowed to roam freely in their cages and sacrificed 1 h post-injection by CO_2 asphyxiation under 2% isoflurane anesthesia. Cardiac puncture was performed immediately after sacrifice to recover blood, and organs of interest were harvested, rinsed with PBS, and blotted dry. Each organ was weighed, and the radioactivity measured using a calibrated γ counter (Packard Cobra II Autogamma counter, PerkinElmer, Waltham, MA, USA) with a 1 min acquisition time per sample. All radioactivity measurements were decay corrected to the time of injection, and the injected dose per gram of tissue (%ID/g) calculated based on measured organ weights, with the exception of blood, bone, and muscle which were scaled in accordance with literature values.[60]

■ ASSOCIATED CONTENT

ⓢ Supporting Information

The Supporting Information is available free of charge at https://pubs.acs.org/doi/10.1021/acs.bioconjchem.2c00038.

> Syntheses, NMR and mass spectra, in vitro cell binding assays, radiolabeling and radiotracer prep data, *ex vivo* biodistribution study results, DFT computation figures and tables, X-ray data (PDF)

■ AUTHOR INFORMATION

Corresponding Author

Chris Orvig − *Medicinal Inorganic Chemistry Group, Department of Chemistry, University of British Columbia, Vancouver, British Columbia V6T 1Z1, Canada;*

ⓘ orcid.org/0000-0002-2830-5493; Email: orvig@
chem.ubc.ca

Authors

Luke Wharton − *Life Sciences Division, TRIUMF, Vancouver, British Columbia V6T 2A3, Canada; Medicinal Inorganic Chemistry Group, Department of Chemistry, University of British Columbia, Vancouver, British Columbia V6T 1Z1, Canada;* ⓘ orcid.org/0000-0002-0636-8741

Chengcheng Zhang − *Department of Molecular Oncology, BC Cancer Research Institute, Vancouver, British Columbia V5Z 1L3, Canada;* ⓘ orcid.org/0000-0001-5786-4748

Hua Yang − *Life Sciences Division, TRIUMF, Vancouver, British Columbia V6T 2A3, Canada; Department of Chemistry, Simon Fraser University, Burnaby, British Columbia V5A 1S6, Canada;* ⓘ orcid.org/0000-0003-1833-9515

Jutta Zeisler − *Department of Molecular Oncology, BC Cancer Research Institute, Vancouver, British Columbia V5Z 1L3, Canada*

Valery Radchenko − *Life Sciences Division, TRIUMF, Vancouver, British Columbia V6T 2A3, Canada; Department of Chemistry, University of British Columbia, Vancouver, British Columbia V6T 1Z1, Canada*

Cristina Rodríguez-Rodríguez − *Faculty of Pharmaceutical Sciences, University of British Columbia, Vancouver, British Columbia V6T 1Z3, Canada; Department of Physics and Astronomy, University of British Columbia, Vancouver, British Columbia V6T 1Z1, Canada;* ⓘ orcid.org/0000-0002-3313-4422

Maryam Osooly − *Faculty of Pharmaceutical Sciences, University of British Columbia, Vancouver, British Columbia V6T 1Z3, Canada*

Brian O. Patrick − *Department of Chemistry, University of British Columbia, Vancouver, British Columbia V6T 1Z1, Canada;* ⓘ orcid.org/0000-0002-2921-8439

Kuo-Shyan Lin − *Department of Molecular Oncology, BC Cancer Research Institute, Vancouver, British Columbia V5Z 1L3, Canada; Department of Radiology, University of British Columbia, Vancouver, British Columbia V5Z 1M9, Canada;* ⓘ orcid.org/0000-0002-0739-0780

François Bénard − *Department of Molecular Oncology, BC Cancer Research Institute, Vancouver, British Columbia V5Z 1L3, Canada; Department of Radiology, University of British Columbia, Vancouver, British Columbia V5Z 1M9, Canada;* ⓘ orcid.org/0000-0001-7995-3581

Paul Schaffer − *Life Sciences Division, TRIUMF, Vancouver, British Columbia V6T 2A3, Canada; Department of Chemistry, Simon Fraser University, Burnaby, British Columbia V5A 1S6, Canada; Department of Radiology, University of British Columbia, Vancouver, British Columbia V5Z 1M9, Canada;* ⓘ orcid.org/0000-0002-6392-8792

Complete contact information is available at:
https://pubs.acs.org/10.1021/acs.bioconjchem.2c00038

Notes

The authors declare no competing financial interest.

◼ REFERENCES

(1) American Cancer Society. Facts & Figures 2020, http://www.cancer.org/cancer/skincancer-melanoma/detailedguide/melanoma-skin-cancer-key-statistics. Accessed January 14 2021.

(2) Dickson, P. V.; Gershenwald, J. E. Staging and Prognosis of Cutaneous Melanoma. *Surg. Oncol. Clin. N. Am.* **2011**, *20*, 1−17.

(3) Leonardi, G. C.; Falzone, L.; Salemi, R.; Zanghì, A.; Spandidos, D. A.; Mccubrey, J. A.; Candido, S.; Libra, M. Cutaneous Melanoma: From Pathogenesis to Therapy (Review). *Int. J. Oncol.* **2018**, *52*, 1071−1080.

(4) Eggermont, A. M. M.; Spatz, A.; Robert, C. Cutaneous Melanoma. *Lancet* **2014**, *383*, 816−827.

(5) Yang, J.; Manson, D. K.; Marr, B. P.; Carvajal, R. D. Treatment of Uveal Melanoma: Where Are We Now? *Therapeutic Advances in Medical Oncology.* **2018**, *10*, 175883401875717.

(6) Kostelnik, T. I.; Orvig, C. Radioactive Main Group and Rare Earth Metals for Imaging and Therapy. *Chem. Rev.* **2019**, *119*, 902−956.

(7) Sadowski, S. M.; Neychev, V.; Millo, C.; Shih, J.; Nilubol, N.; Herscovitch, P.; Pacak, K.; Marx, S. J.; Kebebew, E. Prospective Study of 68Ga-DOTATATE Positron Emission Tomography/Computed Tomography for Detecting Gastro-Entero-Pancreatic Neuroendocrine Tumors and Unknown Primary Sites. *J. Clin. Oncol.* **2016**, *34* (6), 588−597.

(8) Aslani, A.; Snowdon, G. M.; Bailey, D. L.; Schembri, G. P.; Bailey, E. A.; Pavlakis, N.; Roach, P. J. Lutetium-177 DOTATATE Production with an Automated Radiopharmaceutical Synthesis System. *Asia Ocean. J. Nucl. Med. Biol.* **2015**, *3* (2), 107−115.

(9) Alcocer-Ávila, M. E.; Ferreira, A.; Quinto, M. A.; Morgat, C.; Hindié, E.; Champion, C. Radiation Doses from 161Tb and 177Lu in Single Tumour Cells and Micrometastases. *EJNMMI Phys.* **2020**, *7* (1), 1 DOI: 10.1186/s40658-020-00301-2.

(10) Eychenne, R.; Chérel, M.; Haddad, F.; Guérard, F.; Gestin, J. F. Overview of the Most Promising Radionuclides for Targeted Alpha Therapy: The "Hopeful Eight." *Pharmaceutics.* **2021**, *13*, 906.

(11) Ramogida, C. F.; Orvig, C. Tumour Targeting with Radiometals for Diagnosis and Therapy. *Chem. Commun.* **2013**, *49* (42), 4720−4739.

(12) O'Donoghue, J. A.; Bardies, M.; Wheldon, T. E.; Sgouros, G. Relationships between Tumor Size and Curability for Uniformly Targeted Therapy with Beta-Emitting Radionuclides. *J. Nucl. Med.* **1995**, *36* (10), 1902−1912.

(13) Wheldon, T. E.; O'Donoghue, J. A.; Barrette, A.; Michalowski, A. S. The Curability of Tumours of Differing Size by Targeted Radiotherapy Using 131I or 90Y. *Radiother. Oncol.* **1991**, *21* (2), 91−99.

(14) Basunia, M. S. Nuclear Data Sheets for A = 213. *Nucl. Data Sheets* **2007**, *108* (3), 633−680.

(15) De Swart, J.; Chan, H. S.; Goorden, M. C.; Morgenstern, A.; Bruchertseifer, F.; Beekman, F. J.; De Jong, M.; Konijnenberg, M. W. Utilizing High-Energy γ-Photons for High-Resolution 213 Bi SPECT in Mice. *J. Nucl. Med.* **2016**, *57*, 486−492.

(16) van Dijk, B.; Allen, K. J. H.; Helal, M.; Vogely, H. C.; Lam, M. G. E. H.; de Klerk, J. M. H.; Weinans, H.; van der Wal, B. C. H.; Dadachova, E. Radioimmunotherapy of Methicillin-Resistant Staphylococcus Aureus in Planktonic State and Biofilms. *PLoS One* **2020**, *15* (5), e0233086.

(17) Tafreshi, N. K.; Tichacek, C. J.; Pandya, D. N.; Doligalski, M. L.; Budzevich, M. M.; Kil, H. J.; Bhatt, N. B.; Kock, N. D.; Messina, J.

L.; Ruiz, E. E.; Delva, N. C.; Weaver, A.; Gibbons, W. R.; Boulware, D. C.; Khushalani, N. I.; El-Haddad, G.; Triozzi, P. L.; Moros, E. G.; McLaughlin, M. L.; Wadas, T. J.; Morse, D. L. Melanocortin 1 Receptor−Targeted a-Particle Therapy for Metastatic Uveal Melanoma. *J. Nucl. Med.* **2019**, *60*, 1124−1133.

(18) Wolf Horrell, E. M.; Boulanger, M. C.; D'Orazio, J. A. Melanocortin 1 Receptor: Structure, Function, and Regulation. *Front. Genet.* **2016**, *7*, 95.

(19) López, M. N.; Pereda, C.; Ramírez, M.; Mendoza-Naranjo, A.; Serrano, A.; Ferreira, A.; Poblete, R.; Kalergis, A. M.; Kiessling, R.; Salazar-Onfray, F. Melanocortin 1 Receptor Is Expressed by Uveal Malignant Melanoma and Can Be Considered a New Target for Diagnosis and Immunotherapy. *Investig. Ophthalmol. Vis. Sci.* **2007**, *48* (3), 1219−1227.

(20) Zhang, C.; Zhang, Z.; Zeisler, J.; Colpo, N.; Lin, K. S.; Bénard, F. Selective Cyclized α-Melanocyte-Stimulating Hormone Derivative with Multiple N-Methylations for Melanoma Imaging with Positron Emission Tomography. *ACS Omega* **2020**, *5*, 10767−10773.

(21) Zhang, C.; Zhang, Z.; Lin, K. S.; Pan, J.; Dude, I.; Hundal-Jabal, N.; Colpo, N.; Bénard, F. Preclinical Melanoma Imaging with 68Ga-Labeled α-Melanocyte-Stimulating Hormone Derivatives Using PET. *Theranostics* **2017**, *7*, 805−813.

(22) Zhang, C.; Zhang, Z.; Lin, K. S.; Lau, J.; Zeisler, J.; Colpo, N.; Perrin, D. M.; Bénard, F. Melanoma Imaging Using 18 F-Labeled α-Melanocyte-Stimulating Hormone Derivatives with Positron Emission Tomography. *Mol. Pharmaceutics* **2018**, *15* (6), 2116−2122.

(23) Guo, H.; Yang, J.; Gallazzi, F.; Miao, Y. Effects of the Amino Acid Linkers on the Melanoma-Targeting and Pharmacokinetic Properties of 111In-Labeled Lactam Bridge-Cyclized α-MSH Peptides. *J. Nucl. Med.* **2011**, *52*, 608−616.

(24) Xu, J.; Yang, J.; Gonzalez, R.; Fisher, D. R.; Miao, Y. Melanoma-Targeting Property of Y-90-Labeled Lactam-Cyclized α-Melanocyte-Stimulating Hormone Peptide. *Cancer Biother. Radiopharm.* **2019**, *34*, 597−603.

(25) Morais, M.; Oliveira, B. L.; Correia, J. D. G.; Oliveira, M. C.; Jiménez, M. A.; Santos, I.; Raposinho, P. D. Influence of the Bifunctional Chelator on the Pharmacokinetic Properties of 99mTc-(CO)3-Labeled Cyclic α-Melanocyte Stimulating Hormone Analog. *J. Med. Chem.* **2013**, *56* (5), 1961−1973.

(26) Guo, H.; Miao, Y. Introduction of an 8-Aminooctanoic Acid Linker Enhances Uptake of 99mTc-Labeled Lactam Bridge-Cyclized α-MSH Peptide in Melanoma. *J. Nucl. Med.* **2014**, *55* (12), 2057−2063.

(27) Li, H.; Sadler, P. J.; Sun, H. Unexpectedly Strong Binding of a Large Metal Ion (Bi3+) to Human Serum Transferrin. *J. Biol. Chem.* **1996**, *271* (16), 9483−9489.

(28) Montavon, G.; Le Du, A.; Champion, J.; Rabung, T.; Morgenstern, A. DTPA Complexation of Bismuth in Human Blood Serum. *Dalt. Trans.* **2012**, *41* (28), 8615−8623.

(29) Stavila, V.; Davidovich, R. L.; Gulea, A.; Whitmire, K. H. Bismuth(III) Complexes with Aminopolycarboxylate and Polyaminopolycarboxylate Ligands: Chemistry and Structure. *Coord. Chem. Rev.* **2006**, *250*, 2782−2810.

(30) Rosenblat, T. L.; McDevitt, M. R.; Mulford, D. A.; Pandit-Taskar, N.; Divgi, C. R.; Panageas, K. S.; Heaney, M. L.; Chanel, S.; Morgenstern, A.; Sgouros, G.; Larson, S. M.; Scheinberg, D. A.; Jurcic, J. G. Sequential Cytarabine and α-Particle Immunotherapy with Bismuth-213-Lintuzumab (HuM195) for Acute Myeloid Leukemia. *Clin. Cancer Res.* **2010**, *16* (21), 5303−5311.

(31) Poty, S.; Francesconi, L. C.; McDevitt, M. R.; Morris, M. J.; Lewis, J. S. α-Emitters for Radiotherapy: From Basic Radiochemistry to Clinical Studies-Part 2. *J. Nucl. Med.* **2018**, *59* (7), 1020−1027.

(32) Shin, I. S.; Lee, S. M.; Kim, H. S.; Yao, Z.; Regino, C.; Sato, N.; Cheng, K. T.; Hassan, R.; Campo, M. F.; Albone, E. F.; Choyke, P. L.; Pastan, I.; Paik, C. H. Effect of Chelator Conjugation Level and Injection Dose on Tumor and Organ Uptake of 111In-Labeled MORAb-009, an Anti-Mesothelin Antibody. *Nucl. Med. Biol.* **2011**, *38* (8), 1119−1127.

(33) Giannini, G.; Milazzo, F. M.; Battistuzzi, G.; Rosi, A.; Anastasi, A. M.; Petronzelli, F.; Albertoni, C.; Tei, L.; Leone, L.; Salvini, L.; De Santis, R. Synthesis and Preliminary in Vitro Evaluation of DOTA-Tenatumomab Conjugates for Theranostic Applications in Tenascin Expressing Tumors. *Bioorg. Med. Chem.* **2019**, *27* (15), 3248−3253.

(34) Delage, J. A.; Faivre-Chauvet, A.; Barbet, J.; Fierle, J. K.; Schaefer, N.; Coukos, G.; Viertl, D.; Dunn, S. M.; Gnesin, S.; Prior, J. O. Impact of DOTA Conjugation on Pharmacokinetics and Immunoreactivity of [177Lu]Lu-1C1m-Fc, an Anti TEM-1 Fusion Protein Antibody in a TEM-1 Positive Tumor Mouse Model. *Pharmaceutics* **2021**, *13* (1), 96.

(35) Rijpkema, M.; Bos, D. L.; Cornelissen, A. S.; Franssen, G. M.; Goldenberg, D. M.; Oyen, W. J.; Boerman, O. C. Optimization of Dual-Labeled Antibodies for Targeted Intraoperative Imaging of Tumors. *Mol. Imaging* **2015**, *14* (5), 348−355.

(36) Kobayashi, H.; Wu, C.; Yoo, T. M.; Sun, B. F.; Drumm, D.; Pastan, I.; Paik, C. H.; Gansow, O. A.; Carrasquillo, J. A.; Brechbiel, M. W. Evaluation of the in Vivo Biodistribution of Yttrium-Labeled Isomers of CHX-DTPA-Conjugated Monoclonal Antibodies. *J. Nucl. Med.* **1998**, *39*, 829−836.

(37) Spreckelmeyer, S.; Ramogida, C. F.; Rousseau, J.; Arane, K.; Bratanovic, I.; Colpo, N.; Jermilova, U.; Dias, G. M.; Dude, I.; Jaraquemada-Peláez, M. D. G.; Bénard, F.; Schaffer, P.; Orvig, C. P-NO2-Bn-H4neunpa and H4neunpa-Trastuzumab: Bifunctional Chelator for Radiometalpharmaceuticals and 111In Immuno-Single Photon Emission Computed Tomography Imaging. *Bioconjugate Chem.* **2017**, *28*, 2145−2159.

(38) Wharton, L.; Kurakina, E.; Radchenko, V.; Schaffer, P.; Orvig, C. Chemical Promiscuity of Non-Macrocyclic Multidentate Chelating Ligands for Radiometal Ions: H4neunpa-NH2vs H4noneunpa. *Inorg. Chem.* **2021**, *60*, 4076−4092.

(39) Pearson, R. G. Recent Advances in the Concept of Hard and Soft Acids and Bases. *J. Chem. Educ.* **1987**, *64*, 561−567.

(40) Whitmire, K. H. Bismuth: Inorganic Chemistry. In *Encyclopedia of Inorganic and Bioinorganic Chemistry* **2004**, 1−32.

(41) Brechbiel, M. W.; Gansow, O. A.; Pippin, C. G.; Rogers, R. D.; Planalp, R. P. Preparation of the Novel Chelating Agent N-(2-Aminoethyl)-Trans-1,2-Diaminocyclohexane-N,N′,N″-Pentaacetic Acid (H5CyDTPA), a Preorganized Analogue of Diethylenetriaminepentaacetic Acid (H5DTPA), and the Structures of BiIII-(CyDTPA)2- and BiIII(H2DTPA) Com. *Inorg. Chem.* **1996**, *35* (21), 6343−6348.

(42) Milenic, D. E.; Roselli, M.; Mirzadeh, S.; Pippin, C. G.; Gansow, O. A.; Colcher, D.; Brechbiel, M. W.; Schlom, J. In Vivo Evaluation of Bismuth-Labeled Monoclonal Antibody Comparing DTPA-Derived Bifunctional Chelates. *Cancer Biother. Radiopharm.* **2001**, *16* (2), 133−146.

(43) Haiges, R.; Rahm, M.; Dixon, D. A.; Garner, E. B.; Christe, K. O. Binary Group 15 Polyazides. Structural Characterization of [Bi(N 3) 4] -, [Bi(N 3) 5] 2-, [Bipy·Bi(N 3) 5] 2-, [Bi(N 3) 6] 3-, Bipy· As(N 3) 3, Bipy·Sb(N 3) 3, and [(Bipy) 2. *Inorg. Chem.* **2012**, *51* (2), 1127−1141.

(44) Martins, E. P. S.; Rocha, G. B.; Simoni, J. de A.; Espínola, J. G. de P. Synthesis, Thermochemical and Quantum Chemical Studies on Antimony(III)and Bismuth(III)Complexes with 2,2′-Bipyridine and 1,10-Phenanthroline. *Thermochim. Acta* **2019**, *676*, 234−240.

(45) Toma, O.; Mercier, N.; Allain, M.; Forni, A.; Meinardi, F.; Botta, C. Aggregation Induced Phosphorescent N-Oxyde-2,2′-Bipyridine Bismuth Complexes and Polymorphism-Dependent Emission. *Dalt. Trans.* **2015**, *44* (33), 14589−14593.

(46) Toma, O.; Mercier, N.; Allain, M.; Meinardi, F.; Forni, A.; Botta, C. Mechanochromic Luminescence of N, N′-Dioxide-4,4′-Bipyridine Bismuth Coordination Polymers. *Cryst. Growth Des.* **2020**, *20* (12), 7658−7666.

(47) Morgenstern, A.; Bruchertseifer, F.; Apostolidis, C. Bismuth-213 and Actinium-225 − Generator Performance and Evolving Therapeutic Applications of Two Generator-Derived Alpha-Emitting Radioisotopes. *Curr. Radiopharm.* **2012**, *5* (3), 221−227.

(48) Ma, D.; McDevitt, M. R.; Finn, R. D.; Scheinberg, D. A. Breakthrough of 225Ac and Its Radionuclide Daughters from an 225Ac/213 Bi Generator: Development of New Methods, Quantitative Characterization, and Implications for Clinical Use. *Appl. Radiat. Isot.* **2001**, *55* (5), 667−678.

(49) Chan, H. S.; de Blois, E.; Konijnenberg, M. W.; Morgenstern, A.; Bruchertseifer, F.; Norenberg, J. P.; Verzijlbergen, F. J.; de Jong, M.; Breeman, W. A. P. Optimizing Labelling Conditions of 213 Bi-DOTATATE for Preclinical Applications of Peptide Receptor Targeted Alpha Therapy. *EJNMMI Radiopharm. Chem.* **2017**, *1* (1), 1 DOI: 10.1186/s41181-016-0014-4.

(50) Li, L.; Jaraquemada-Peláez, M. D. G.; Kuo, H. T.; Merkens, H.; Choudhary, N.; Gitschtaler, K.; Jermilova, U.; Colpo, N.; Uribe-Munoz, C.; Radchenko, V.; Schaffer, P.; Lin, K. S.; Bénard, F.; Orvig, C. Functionally Versatile and Highly Stable Chelator for 111In and 177Lu: Proof-of-Principle Prostate-Specific Membrane Antigen Targeting. *Bioconjugate Chem.* **2019**, *30*, 1539−1553.

(51) Robertson, A. K. H.; McNeil, B. L.; Yang, H.; Gendron, D.; Perron, R.; Radchenko, V.; Zeisler, S.; Causey, P.; Schaffer, P. 232Th-Spallation-Produced 225Ac with Reduced 227Ac Content. *Inorg. Chem.* **2020**, *59* (17), 12156−12165.

(52) Frisch, M. J.; Trucks, G. W.; Schlegel, H. B.; Scuseria, G. E.; Robb, M. A.; Cheeseman, J. R.; Scalmani, G.; Barone, V.; Petersson, G. A.; Nakatsuji, H.; Li, X.; Caricato, M.; Marenich, A. V.; Bloino, J.; Janesko, B. G.; Gomperts, R.; Mennucci, B.; Hratchian, H. P.; Ortiz, J. V.; Izmaylov, A. F.; Sonnenberg, J. L.; Williams-Young, D.; Ding, F.; Lipparini, F.; Egidi, F.; Goings, J.; Peng, B.; Petrone, A.; Henderson, T.; Ranasinghe, D.; Zakrzewski, V. G.; Gao, J.; Rega, N.; Zheng, G.; Liang, W.; Hada, M.; Ehara, M.; Toyota, K.; Fukuda, R.; Hasegawa, J.; Ishida, M.; Nakajima, T.; Honda, Y.; Kitao, O.; Nakai, H.; Vreven, T.; Throssell, K.; Montgomery, J. A., Jr.; Peralta, J. E.; Ogliaro, F.; Bearpark, M. J.; Heyd, J. J.; Brothers, E. N.; Kudin, K. N.; Staroverov, V. N.; Keith, T. A.; Kobayashi, R.; Normand, J.; Raghavachari, K.; Rendell, A. P.; Burant, J. C.; Iyengar, S. S.; Tomasi, J.; Cossi, M.; Millam, J. M.; Klene, M.; Adamo, C.; Cammi, R.; Ochterski, J. W.; Martin, R. L.; Morokuma, K.; Farkas, O.; Foresman, J. B.; Fox, D. J. *Gaussian 16, Rev. B.01.*; Gaussian, Inc.: Wallingford, CT, 2016.

(53) Stoll, H.; Metz, B.; Dolg, M. Relativistic Energy-Consistent Pseudopotentials - Recent Developments. *J. Comput. Chem.* **2002**, *23* (8), 767−778.

(54) Hanwell, M. D; Curtis, D. E; Lonie, D. C; Vandermeersch, T.; Zurek, E.; Hutchison, G. R Avogadro: An Advanced Semantic Chemical Editor, Visualization, and Analysis Platform. *J. Cheminform.* **2012**, *4* (8), 1 DOI: 10.1186/1758-2946-4-17.

(55) Glendening, E. D.; Reed, A. E.; Carpenter, J. E.; Weinhold, F. NBO 3.0. *QCPE Bull.* **1990**, *10*, 1.
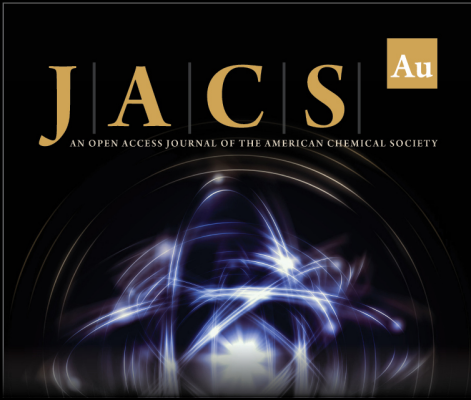
(56) *SAINT, V8.40B*; Bruker AXS Inc., Madison, WI, 2013.

(57) Sheldrick, G. M. Crystal Structure Refinement with SHELXL. *Acta Crystallogr. Sect. C Struct. Chem.* **2015**, *71*, 3−8.

(58) Dolomanov, O. V.; Bourhis, L. J.; Gildea, R. J.; Howard, J. A. K.; Puschmann, H. OLEX2: A Complete Structure Solution, Refinement and Analysis Program. *J. Appl. Crystallogr.* **2009**, *42* (2), 339−341.

(59) Branderhorst, W.; Vastenhouw, B.; Beekman, F. J. Pixel-Based Subsets for Rapid Multi-Pinhole SPECT Reconstruction. *Phys. Med. Biol.* **2010**, *55* (7), 2023−2034.

(60) Foster, H. L.; Small, J. D.; Fox, J. G. *The Mouse in Biomedical Research*; Academic Press: New York, 1983.